Inorganic Chemistry

pubs.acs.org/IC

Article

Impact of the Anthryl Linking Mode on the Photophysics and Excited-State Dynamics of Re(I) Complexes [ReCl(CO)$_3$(4′-An-terpy-κ^2N)]

Magdalena Małecka, Agata Szlapa-Kula, Anna M. Maroń, Przemyslaw Ledwon, Mariola Siwy, Ewa Schab-Balcerzak, Karolina Sulowska, Sebastian Maćkowski, Karol Erfurt, and Barbara Machura*

Cite This: *Inorg. Chem.* 2022, 61, 15070−15084

Read Online

ACCESS | Metrics & More | Article Recommendations | Supporting Information

ABSTRACT: Rhenium(I) complexes with 2,2′:6′,2″-terpyridines (terpy) substituted with 9-anthryl (**1**) and 2-anthryl (**2**) were synthesized, and the impact of the anthryl linking mode on the ground- and excited-state properties of resulting complexes [ReCl(CO)$_3$(4′-An-terpy-κ^2N)] (An—anthryl) was investigated using a combination of steady-state and time-resolved optical techniques accompanied by theoretical calculations. Different attachment positions of anthracene modify the overlap between the molecular orbitals and thus the electronic coupling of the anthracene and {ReCl(CO)$_3$(terpy-κ^2N)} chromophores. Following the femtosecond transient absorption, the lowest triplet excited state of both complexes was found to be localized on the anthracene chromophore. The striking difference between **1** and **2** concerns the triplet-state formation dynamics. A more planar geometry of 2-anthryl-terpy (**2**), and thus better electronic communication between the anthracene and {ReCl(CO)$_3$(terpy-κ^2N)} chromophores, facilitates the formation of the ^{3}An triplet state. In steady-state photoluminescence spectra, the population ratio of ^{3}MLCT and ^{3}An was found to be dependent not only on the anthryl linking mode but also on solvent polarity and excitation wavelengths. In dimethyl sulfoxide (DMSO), compounds **1** and **2** excited with λ_{exc} > 410 nm show both ^{3}MLCT and ^{3}An emissions, which are rarely observed. Additionally, the abilities of the designed complexes for $^1O_2$ generation and light emission under the external voltage were preliminary examined.

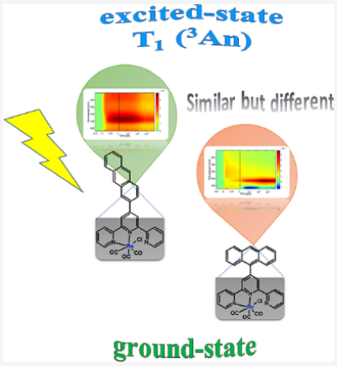

INTRODUCTION

Since the first report on Re(I) carbonyl diamine complexes by Wrighton and Morse,[1] a large number of experimental and theoretical studies have been carried out to understand the ground- and excited-state properties of [Re(CO)$_3$X(N^N)]$^{n+}$ (X—ancillary ligand, n = 0 or 1). Structural modifications of the chelating organic ligand (N^N) and variations of the ancillary one (X = halogens, carboxylates, phosphines, nitriles, isonitriles, etc.) have been found to be effective tools for fine-tuning the metal-to-ligand charge-transfer (MLCT) state of these systems or switching it to ligand-to-ligand charge transfer (LLCT), halogen-to-ligand charge transfer (XLCT), intraligand charge transfer (ILCT), intraligand (IL), and σ-bond-to-ligand charge transfer (SBLCT) ones.[2−8] Relatively simple synthetic procedure, thermal stability, and photophysical properties make Re(I) carbonyl polypyridyl complexes very promising agents for bioimaging and photodynamic therapy (PDT) of cancer,[9−18] organic light-emitting diodes (OLED),[19−23] and photocatalysis for selective reduction of CO_2 to CO.[24−29] The control of electronically excited states in [Re(CO)$_3$X(N^N)]$^{n+}$ systems, and thus the ability to tune their photophysical properties in the context of such many applications, is generally realized by the manipulation of the diimine core, substitution of the diimine ligand with π-conjugated organic chromophores, electron-donating or -withdrawing substituents, and variations of the ancillary X ligand.[1−29] More specifically, Re(I) carbonyl chromophores with prolonged excited-state lifetimes have been successfully obtained using two popular concepts: (i) via the attachment of π-conjugated organic chromophores to the diimine ligand and formation of bichromophoric systems featuring the triplet-state equilibrium between ^{3}MLCT and ^{3}IL,[30−32] and (ii) via introduction of electron-rich groups into the diimine unit and switching the emitting state from ^{3}MLCT to ^{3}ILCT.[33,34] Excellent examples of such systems are Re(I) complexes with *N*-(1,10-phenanthroline)-4-(1-piperidinyl)naphthalene-1,8-dicarboximide[30] and 1,10-phenanthroline substituted with triphenylamine at the 5-position,[33] with approximately 3000-fold and 30-fold longer excited-state lifetimes compared to the parent complex [ReCl(CO)$_3$(phen)], respectively. Dramatic enhancement of the excited-state lifetime has also been reported among terpyridine Re(I) systems. As a result of the

Received: June 21, 2022
Published: September 14, 2022

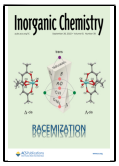

https://doi.org/10.1021/acs.inorgchem.2c02160
Inorg. Chem. 2022, 61, 15070−15084

Scheme 1. Structural Formulas of Re(I) Complexes Investigated in This Study

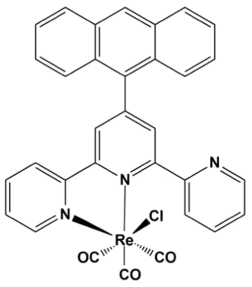

1
$[ReCl(CO)_3(4'\text{-}(9\text{-anthryl})\text{-terpy-}\kappa^2N)]$

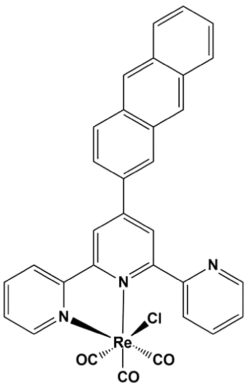

2
$[ReCl(CO)_3(4'\text{-}(2\text{-anthryl})\text{-terpy-}\kappa^2N)]$

decoration of C_6H_5-terpy with the dimethylamine group and formation of the ^{3}ILCT excited state in $[ReCl(CO)_3(Me_2N\text{-}C_6H_4\text{-terpy-}\kappa^2N)]$, the lifetime of the resulting complex became ca. 260 times longer than that for $[ReCl(CO)_3(C_6H_5\text{-terpy-}\kappa^2N)]$ with the lowest triplet state of the ^{3}MLCT character.[34]

In our recent work,[35] we investigated the impact of selected π-conjugated aryl chromophores on the photophysical behavior of $[ReCl(CO)_3(4'\text{-}Ar^n\text{-terpy-}\kappa^2N)]$. We demonstrated that Re(I) complexes with 2,2′:6′,2″-terpyridines (terpy) substituted with 1-naphthyl-, 2-naphthyl-, and 9-phenanthryl are typical ^{3}MLCT emitters, and naphthyl- and phenanthryl substituents have a negligible effect on the energies of the ^{1}MLCT absorption and ^{3}MLCT emission bands. On the contrary, the attachment of the electron-rich pyrenyl group leads to a bathochromic shift of the visible absorption accompanied by a significant increase in its intensity relative to the parent complex $[ReCl(CO)_3(terpy\text{-}\kappa^2N)]$,[36,37] as well as substantial enhancement of the room-temperature (RT) photoluminescence lifetime of $[ReCl(CO)_3(4'\text{-}(1\text{-pyrenyl})\text{-terpy-}\kappa^2N)]$ (4.4 μs) in comparison to $[ReCl(CO)_3(terpy\text{-}\kappa^2N)]$ (3 ns) due to the establishment of the triplet-state equilibrium between the pyrenyl and Re(I) coordination framework. Further, we demonstrated that the excitation of $[ReCl(CO)_3(4'\text{-pyrenyl-terpy-}\kappa^2N)]$ populates predominately the ^{1}ILCT state, which undergoes the energy transfer to the ^{1}MLCT* state via the Förster resonance energy transfer (FRET) mechanism. The ^{1}MLCT state formed in this process is transformed into ^{3}MLCT* by femtosecond intersystem crossing (ISC). In the next step, triplet−triplet energy transfer occurs from the relaxed ^{3}MLCT state to a lower energy ^{3}IL/^{3}ILCT state localized on the pyrenyl-terpy ligand.

Continuing exploration of this field, two Re(I) complexes with 2,2′:6′,2″-terpyridines (terpy) substituted with 9-anthryl (**1**) and 2-anthryl (**2**) were synthesized to investigate the impact of the anthryl group and its linking mode on the ground- and excited-state properties of resulting complexes $[ReCl(CO)_3(4'\text{-An-terpy-}\kappa^2N)]$ (Scheme 1). In similarity to pyrene, the anthracene chromophore (An) is well known for its valuable optical and electronic properties. Its attachment to polypyridyl ligands may lead to the energy transfer from ^{3}MLCT to a long-lived ^{3}IL excited state or, if ^{3}MLCT and ^{3}IL states have similar energies, formation of an excited-state equilibrium in metal complexes.[38−45] Anthracene is also a rare example of a compound, which shows ISC via the upper excited state, that is T_2, which is isoenergetic to the S_1 state.[46,47]

Most remarkably, the only difference between designed complexes **1** and **2** is the relative orientation of anthracene and $\{ReCl(CO)_3(terpy\text{-}\kappa^2N)\}$ chromophores, which was achieved by appending anthracene via its 9-position or 2-position to the terpy ligand. Therefore, by elimination of additional structural factors, this unique pair gives the opportunity to explore the impact of the mutual chromophore orientation and thus their electronic communication on light-triggered processes in such bichromophoric systems. The optimization of the photophysical properties of transition metal complexes by spatial effects still remains a great challenge, and comprehensive studies in this area are strongly desirable for the rational design of new photoluminescent materials with predefined photophysical properties.

In the present work, an insight into the ground- and excited-state properties of **1** and **2** was achieved using a combination of steady-state and time-resolved optical techniques accompanied by theoretical calculations. In addition, the abilities of the designed complexes for $^1O_2$ generation and light emission under the external voltage were preliminary examined.

EXPERIMENTAL SECTION

Materials. The ligands 9-anthryl-terpy and 2-anthryl-terpy were prepared according to the literature method.[48] $Re(CO)_5Cl$, solvents for synthesis (of reagent grade) and for spectroscopic studies (of high-performance liquid chromatography (HPLC) grade), diphenylisobenzofuran (DPBF), $[Ru(bipy)_3](PF_6)_2$, poly(9-vinylcarbazole) (PVK, M_n = 25 000−50 000; Sigma-Aldrich), poly(3,4-(ethylenedioxy)thiophene):poly-(styrenesulfonate) (PEDOT:PSS) (0.1−1.0 S·cm^{-1}), and substrates with pixilated indium tin oxide (ITO) anodes (Ossila) were all commercially available and used without further purification.

Preparation of $[ReCl(CO)_3(4'\text{-}(9\text{-anthryl})\text{-terpy-}\kappa^2N)]$ (1) and $[ReCl(CO)_3(4'\text{-}(2\text{-anthryl})\text{-terpy})]$ (2). The corresponding 4′-(anthracen-9-yl)-2,2′:6′,2″-terpyridine (9-anthryl-terpy) or 4′-(anthracen-2-yl)-2,2′:6′,2″-terpyridine (2-anthryl-terpy) ligand (0.27 mmol) was added to a suspension of $[Re(CO)_5Cl]$ (0.27 mmol) and toluene (35 mL). The reaction mixture was heated at reflux for 8 h under an argon atmosphere. The formed precipitate was filtered off and washed with diethyl ether, dried in the air, and then purified by repeated recrystallization from toluene.

https://doi.org/10.1021/acs.inorgchem.2c02160
Inorg. Chem. 2022, 61, 15070−15084

*[ReCl(CO)$_3$(4′-(9-anthryl)-terpy-κ^{2}N)] (**1**).* Yield: 80%. ^{1}H NMR (400 MHz, dimethyl sulfoxide (DMSO)) δ 9.14 (d, J = 5.2 Hz, 1H, H^{C1}), 9.06 (s, 1H, H^{D8}), 8.90−8.84 (m, 2H, $H^{B4,C4}$), 8.78 (d, J = 4.5 Hz, 1H, H^{A1}), 8.31−8.21 (m, 3H, $H^{C3,D3,D13}$), 8.07−7.97 (m, 3H, $H^{B2,D6,D10}$), 7.79−7.75 (m, 1H, H^{C2}), 7.73 (d, J = 8.9 Hz, 1H, H^{A4}), 7.65−7.47 (m, 6H, $H^{A2,A3,D4,D5,D11,D12}$). ^{13}C NMR (100 MHz, DMSO) δ 197.74 (C^{CO}), 194.54 (C^{CO}), 191.20 (C^{CO}), 161.16 (C^{B1}), 157.35 (C^{A5}), 157.26 (C^{B5}), 156.36 (C^{C5}), 152.83 (C^{C1}), 150.96 (C^{D1}), 149.19 (C^{A1}), 140.03 (C^{C3}), 137.31 (C^{B3}), 136.88 (C^{B2}), 131.26 (C^{D2}), 130.72 (C^{D7}), 130.68 (C^{D9}), 129.54 (C^{D3}), 128.74 (C^{D14}), 128.66 (C^{D6}), 128.60 (C^{D10}), 128.41 (C^{C4}), 127.45 (C^{C2}), 127.07 (C^{D4}), 126.92 (C^{D5}), 126.15 (C^{D8}), 125.68 (C^{D12}), 125.66 (C^{D11}), 125.51 (C^{A4}), 125.46 (C^{B4}), 125.27 (C^{D13}), 125.04 (C^{A3}), 124.79 (C^{A2}). IR (KBr, cm^{-1}): 2023 (vs), 1926 (vs) and 1896 (vs) ν(C≡O); 1611 (m), ν(C═N) and ν(C═C). High-resolution mass spectrometry (HRMS) (electrospray ionization (ESI)) (m/z): $[M - Cl]^+$ calcd for $[C_{32}H_{19}N_3O_3Re]^+$ 680.0984. Found 680.0987. Anal. Calcd for $C_{32}H_{19}ClN_3O_3Re$ (715.17 g·mol^{-1}): C, 53.74; H, 2.68; N, 5.88. Found: C, 53.65; H, 2.74; N, 5.80.

*[ReCl(CO)$_3$(4′-(2-anthryl)-terpy)] (**2**).* Yield: 75%. ^{1}H NMR (400 MHz, DMSO) δ 9.28 (s, 1H), 9.17 (d, J = 8.3 Hz, 1H), 9.10−9.07 (m, 2H), 8.83 (d, J = 4.8 Hz, 1H), 8.77 (s, 1H), 8.70 (s, 1H), 8.46−8.39 (m, 2H), 8.35−8.28 (m, 2H), 8.16 (t, J = 8.2 Hz, 2H), 8.09 (t, J = 7.5 Hz, 1H), 7.96 (d, J = 7.7 Hz, 1H), 7.80 (t, J = 6.6 Hz, 1H), 7.68−7.63 (m, 1H), 7.63−7.56 (m, 2H). ^{13}C NMR: not recorded due to insufficient complex solubility. IR (KBr, cm^{-1}): 2021 (vs), 1915 (vs) and 1893 (vs) ν(C≡O); 1611 (m), ν(C═N) and ν(C═C). HRMS (ESI) (m/z): $[M - Cl]^+$ calcd for $[C_{32}H_{19}N_3O_3Re]^+$ 680.0984. Found 680.0986. Anal. Calcd for $C_{32}H_{19}ClN_3O_3Re·2H_2O$ (751.17 g·mol^{-1}): C, 51.16; H, 3.09; N, 5.59. Found: C, 51. 34; H, 2.83; N, 5.45.

Physical Measurements. High-resolution mass spectrometry analyses were performed on a Waters Xevo G2 Q-TOF mass spectrometer (Waters Corporation) equipped with an ESI source operating in positive-ion modes. Elemental analysis was recorded on a Vario EL Cube apparatus. IR spectra were measured using a Nicolet iS5 Fourier transform infrared (FTIR) spectrophotometer (4000−400 cm^{-1}) in the form of KBr pellets. Absorption spectra were recorded on a Thermo Scientific Evolution 220 (solution) and a Jasco V-570 (solid state as a film deposited on a glass substrate and as blends with poly(*N*-vinylcarbazole) (PVK): 2-(4-*tert*-butylphenyl)-5-(4-biphenylyl)-1,3,4-oxadiazole (PBD) on a glass substrate). NMR spectra were recorded on a Bruker Avance 400 NMR spectrometer (298 K) using DMSO-d_6 as the solvent. Resonance frequencies of 400 and 100 MHz were used for ^{1}H NMR and ^{13}C NMR spectra, respectively.

Cyclic voltammetry (CV) experiments were carried out in a classic three-electrode system. A Pt wire and a Pt spiral were used as working and counter electrodes, respectively. A leakless Ag/AgCl electrode (eDAQ) was used as a reference electrode. The electrode potential was calibrated against ferrocene. Bu_4NPF_6 in CH_2Cl_2 with a concentration of 0.1 mol·dm^{-3} was used as a supporting electrolyte. Measurements were performed with an Autolab PGSTAT 100N with a scan rate of 50 mV·s^{-1}.

Photo- (PL) and Electroluminescence (EL) spectra. Steady-state luminescence spectra were recorded on an FLS-980 fluorescence spectrophotometer equipped with a 450 W Xe lamp and a high-gain photomultiplier PMT + 500 nm (Hamamatsu, R928P) detector. The emission spectra at 77 K were registered in a butyronitrile rigid matrix. The PL lifetime measurements were performed with the time-correlated single photon counting (TCSPC) method. The TCSPC measurements were carried out in optically diluted solutions using a picosecond laser diode (EPL 405 nm) as the excitation light source and PMT (Hamamatsu, R928P, Japan) as a detector. The IRF was designated using the Ludox solution. Decay curves were fitted using deconvolution fit analysis. For samples with long-lived phosphorescence, PL lifetime measurements were performed with the multichannel scaling (MCS) method, and a 60 W microsecond Xe flash lamp was used for sample excitation. The quantum yields of fluorescence were determined by the absolute method using the integrating sphere with the solvent (for argon-saturated solution samples) or the Spectralon reflectance standard (for powdered samples) as blanks. FLS-980 software was used to perform the emission correction and calculation of the quantum yield. To collect electroluminescence (EL) spectra, a precise voltage supply (Gw Instek PSP-405) with the sample fixed to an *XYZ* stage was applied. Light from the OLED device was collected through a 30 mm lens, focused on the entrance slit (50 μm) of a monochromator (Shamrock SR-303i), and detected using a charge-coupled device (CCD) detector (Andor iDus 12305). Typical acquisition times were equal to 10 s. The prealignment of the setup was done using a 405 nm laser.

Singlet oxygen generation efficiency was determined by monitoring the photooxidation of 1,3-diphenylisobenzofuran (DPBF) sensitized by Re(I) complexes in DMSO. Singlet oxygen quantum yields (Φ_Δ) of Re(I) complexes were estimated using $[Ru(bipy)_3](PF_6)_2$ as the standard ($\Phi_{\Delta O_2}$ = 0.66 in DMSO).[49,50]

Femtosecond Transient Absorption (fsTA). Femtosecond TA spectra were recorded using a pump−probe transient absorption spectroscopy system (Ultrafast Systems, Helios) described in our previous work.[35] TA experiments were carried out for the solution samples (in $CHCl_3$, MeCN, and DMSO), stirred during the experiments to avoid photoproduct interference. The absorbance range was equal to 0.20−0.70 in the pumping wavelengths (corresponding to a concentration of 2.5 × 10^{-4} mol·dm^{-3}). The 405 and 355 nm pump pulses were used to excite the samples. Transient absorption data were analyzed using Surface Xplorer (Ultrafast Systems) and OPTIMUS software.[51,52] A more detailed description of the fsTA studies is given in Figures S20−S25 in the Supporting Information (SI).

Computational Details. Theoretical calculations were performed using the Gaussian 09 program package[53] at the density functional theory (DFT) or time-dependent (TD)-DFT level with the PBE1PBE[54,55] hybrid exchange−correlation functional, the def2-TZVPD basis set for rhenium, and the def2-TZVP basis set for other elements.[56,57] In all calculations, the acetonitrile solvent environment was simulated using the polarizable continuum model (PCM).[58,59]

RESULTS AND DISCUSSION

Synthesis, Molecular Structures, and Stability. The complexes [ReCl(CO)$_3$(4′-An-terpy-κ^{2}N)] (An = 9-anthryl (**1**) and 2-anthryl (**2**)) were obtained in satisfactory yields by reacting 4′-An-terpy with $[Re(CO)_5Cl]$ under reflux in toluene. The identity and purity of **1** and **2** were determined by NMR spectroscopy (Figures S1 and S2), FTIR technique (Figures S3 and S4), HRMS (Figures S5 and S6), and elemental analysis. ^{1}H NMR spectra of complexes **1** and **2** demonstrate the splitting of signals for the protons of the peripheral pyridine rings, which confirms the κ^{2}N coordination of the 4′-An-terpy ligand. For **1**, the full assignment of ^{1}H and ^{13}C NMR signals was provided with the aid of two-dimensional techniques ^{1}H−^{1}H correlated spectroscopy (COSY), ^{1}H−^{13}C heteronuclear multiple quantum correlation (HMQC), and ^{1}H−^{13}C heteronuclear multiple bond correlation (HMBC) (Figures S1 and S2). The facial geometry of carbonyl ligands in **1** and **2** was evidenced by solid-state IR spectroscopy, where the characteristic band pattern for CO vibrations was observed. Namely, a sharp intense C≡O stretching band (2024 cm^{-1} for **1** and 2021 cm^{-1} for **2**) was present in the spectra along with two poorly resolved bands in the lower energy range (1927 and 1897 cm^{-1} for **1** and 1916 and 1893 cm^{-1} for **2**; Figures S3 and S4).[1−8,35]

Both Re(I) complexes are stable in solution (Figure S7) and show acceptable photostability (Figure S8).

Regarding the thermal properties, the complexes showed melting temperatures of 177 and 217 °C for **1** and **2**, respectively, as detected using the differential scanning

https://doi.org/10.1021/acs.inorgchem.2c02160
Inorg. Chem. 2022, 61, 15070−15084

calorimetry (DSC) technique. These values are relatively high. After rapid cooling, the compounds form a stable amorphous phase with glass transition registered during the second heating scan at 206 and 198 °C for **1** and **2**, respectively.

Ground-State Properties. To determine the impact of the anthryl molecular geometry on the ground-state properties of [ReCl(CO)$_3$(4′-An-terpy-κ^2N)], complexes **1** and **2** were investigated by cyclic voltammetry and absorption spectroscopy.

The basic electrochemical parameters, such as oxidation onset potential ($E_{ox\ onset}$), reduction onset potential ($E_{red\ onset}$), ionization potential (IP), and electron affinity (EA) are summarized in Table 1. Cyclic voltammetry curves of **1** and **2** are shown in Figure 1. Bu_4NPF_6/CH_2Cl_2 was chosen as an electrolyte due to the good solubility of the studied compounds in this solvent. Both complexes present multistage oxidation and reduction characteristics.

Table 1. Electrochemical Properties of Complexes 1 and 2

	$E_{ox\ onset}$[a] (V)	$E_{red\ onset}$[b] (V)	IP[c] (eV)	EA[d] (eV)	Eg_{el}[e] (eV)	Eg_{opt}[f] (eV)
1	0.67	−1.76	5.77	3.34	2.43	2.61
2	0.61	−1.69	5.71	3.41	2.30	2.46

[a]$E_{ox\ onset}$: oxidation onset potential. [b]$E_{red\ onset}$: reduction onset potential. [c]IP: ionization potential estimated from the equation IP = |e$^-$|(5.1 + $E_{ox\ onset}$). [d]EA: electron affinity estimated from the equation EA = |e$^-$|(5.1 + $E_{red\ onset}$). [e]Eg_{el}: electrochemical band gap estimated from the equation $\Delta Eg_{el} = E_{ox\ onset} - E_{red\ onset}$. [f]$Eg_{opt} = \frac{1240}{\lambda_{onset}}$.

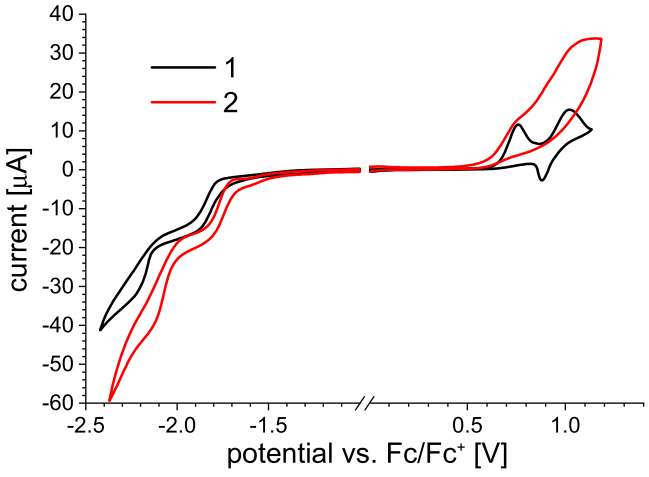

Figure 1. Cyclic voltammetry curves of complexes **1** and **2**. Concentration: 2 mmol·dm^{-3}, electrolyte: Bu_4NPF_6/CH_2Cl_2, and scan rate: 50 mV·s^{-1}.

By analyzing the values of IP and EA, which are related to the removal of an electron from the highest occupied molecular orbital (HOMO) or the addition of an electron to the lowest unoccupied molecular orbital (LUMO), slight differences between **1** and **2** can be noticed. Most remarkably, complex **2** exhibits a narrower electrochemical band gap (Eg_{el}), indicating the increase of the effective coupling in comparison to complex **1**. This is in line with the results of the DFT calculations discussed below and optical energy gap values (Table 1). Similar relationships were also reported for other complexes containing anthracene-based ligands, for example bis(benzo[*h*]quinolinato) Ir(III) complexes[60] and anthracene-bridged bimetallic ruthenium vinyl complexes.[61]

For both complexes, the shape of CV curves indicates the electrochemical irreversibility of reduction and oxidation processes. A noticeable impact of the anthryl linking mode on the shape of the CV recorded during the oxidation leads to the assumption that the HOMO is largely associated with the anthracene substituent. On the other hand, weaker dependence of the reduction process on the anthryl molecular geometry may indicate that the LUMO of these systems is located predominantly on the terpy core.

The electronic absorption spectra of **1** and **2** were recorded in solvents of different polarities and as thin films (Table S1 and Figure 2).

A comparison of spectral features of **1** and **2** in a lower energy region (330−470 nm) clearly indicates that the anthryl linking mode has a noticeable impact on the absorption properties of [ReCl(CO)$_3$(4′-An-terpy-κ^2N)]. For complex **1**, the absorption in this region is in principle a sum of $\pi_{An} \rightarrow \pi^*_{An}$ and Re → terpy* transitions. The structured absorption in the range of 330−390 nm is typical of that of anthracene, while ^{1}MLCT (Re → terpy*) charge transfer contribution is visible in the form of a low-energy shoulder above 390 nm.[41,62,63] These observations are supportive of the weak electronic coupling between the 9-anthryl and terpy units owing to the strong steric hindrance of the rotation about the C−C linker in 9-anthryl-terpy.[48,64] On the contrary, complex **2** does not show typical anthracene-like absorption with clear vibronic progression. In agreement with a more coplanar geometry and thus more extended delocalization of 2-anthryl-terpy, the ^{1}MLCT/^{1}IL$_{An}$ absorption band of **2** shifts to lower energies and becomes slightly more intense compared to that of **1**.[48,64,65] A bathochromic shift of the lowest energy absorption of **1** and **2** caused by replacing acetonitrile with less polar chloroform is due to negative solvatochromism, which is well recognized for rhenium(I) tricarbonyl diimine complexes.[35,66−70] Intensive bands in the high-energy region of **1** and **2** are attributed to $\pi-\pi^*$(terpy) and $\pi-\pi^*$(anthracene) transitions (Figure S9).

The impact of the anthryl group directly attached to the terpy core via its 9-position (**1**) and 2-position (**2**) on the electronic structure of [ReCl(CO)$_3$(4′-An-terpy-κ^2N)] was also investigated theoretically at the DFT/PBE0/def2-TZVPD/def2-TZVP level. The geometry optimization shows good agreement with previously reported experimental X-ray data for structurally related Re(I) complexes.[35,68,70−73] The 9-anthryl and 2-anthryl groups introduced in the terpy ligand do not generate any noticeable structural changes in the {ReClN$_2$C$_3$} coordination core. The bond lengths and bond angles around the Re(I) ion are almost the same for **1** and **2** (Table S2). Also, the electrochemical data of **1** and **2** are satisfactorily reproduced by the calculated ionization potentials and electronic affinities[74] (Table S3). The striking difference between **1** and **2** concerns the dihedral angle between the plane of the anthryl group and the central pyridine ring (72° for **1** and 32° for **2**).

For both compounds, the lowest unoccupied molecular orbital (LUMO) largely resides on the terpy core and the highest occupied molecular orbital (HOMO) is localized on the anthryl substituent, while HOMO−1, HOMO−2, and HOMO−3 orbitals spread over the {Re(CO)$_3$Cl} moiety (Figures 3 and S10). Depending on the anthryl linking mode, no clear energy variations are observed for HOMO, HOMO−

https://doi.org/10.1021/acs.inorgchem.2c02160
Inorg. Chem. 2022, 61, 15070−15084

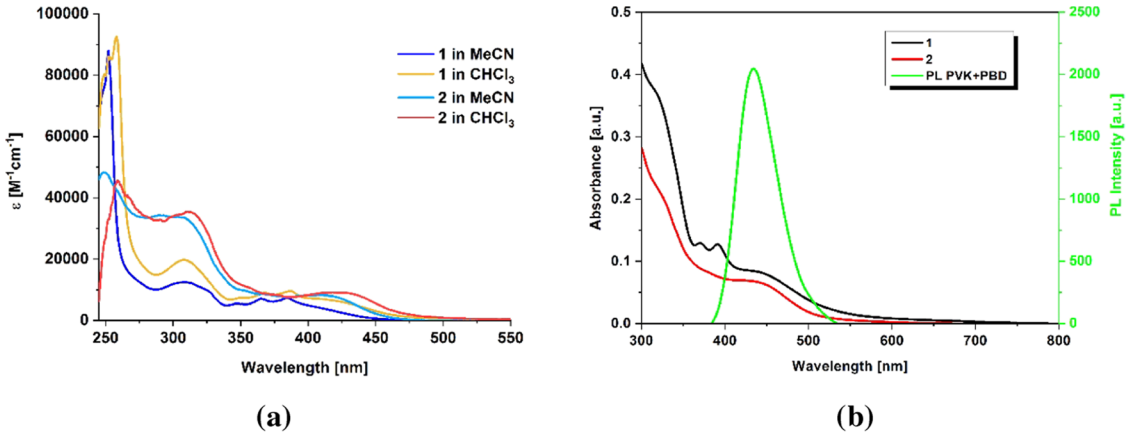

Figure 2. UV−vis absorption spectra of **1** and **2** in solutions (a) and as thin films (b).

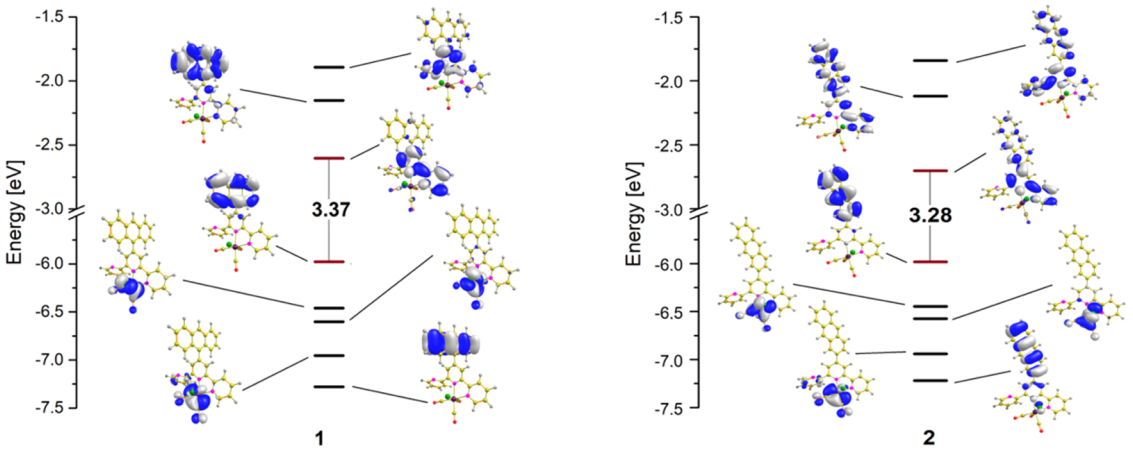

Figure 3. Partial molecular orbital energy-level diagrams for compounds **1** and **2**.

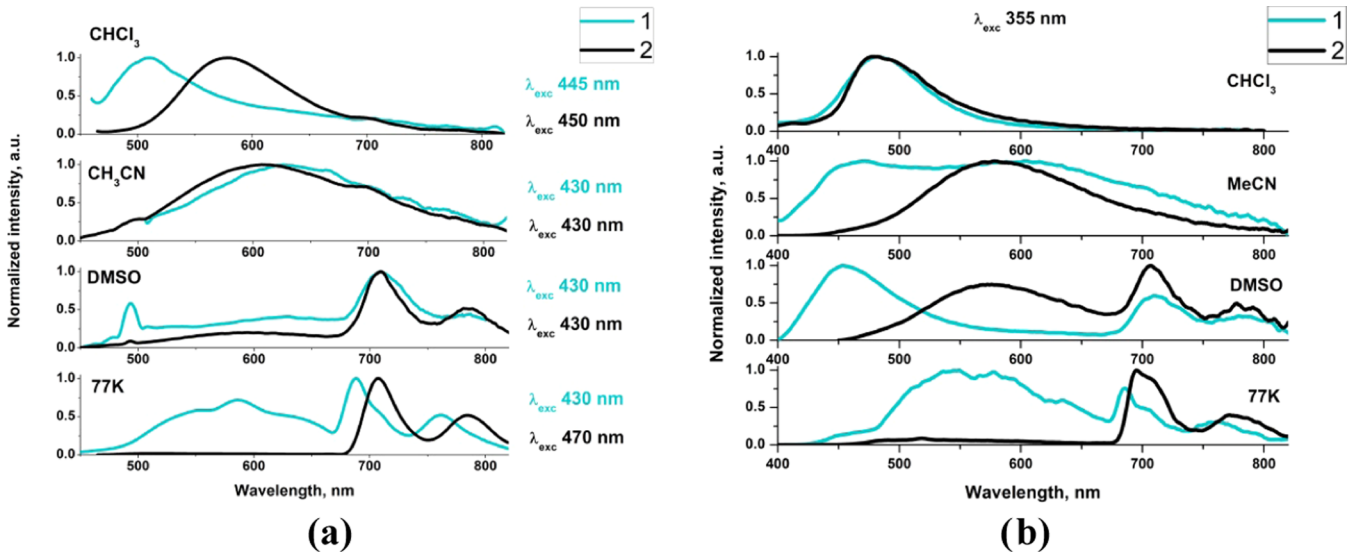

Figure 4. Photoluminescence spectra of **1** and **2** in different environments upon excitation at the red side of the lowest energy absorption (a) and 355 nm (b).

1, HOMO−2, and HOMO−3 energy levels between compounds **1** and **2**. When considering the LUMO levels of **1** and **2**, the replacement of 9-anthryl by 2-anthryl leads to a slight stabilization of the LUMO and thus causes a decrease in the HOMO−LUMO gap of **2** (3.28 eV) relative to **1** (3.37 eV). These changes can be rationalized as resulting from a more coplanar geometry of 2-anthryl-terpy, which leads to a stronger coupling between the 2-anthryl group and the terpy core. As a result of more extended overlapping orbitals of the 2-anthryl and terpy moieties, molecular orbitals LUMO+1 and

https://doi.org/10.1021/acs.inorgchem.2c02160
Inorg. Chem. 2022, 61, 15070−15084

Table 2. Summary of the Photoluminescence Properties of Complexes 1 and 2[a]

	$CHCl_3$				MeCN				DMSO				$CH_3OH:C_2H_5OH$ (77 K)		
	λ_{exc} (nm)	λ_{em} (nm)	τ_{av} (ns)	φ (%)	λ_{exc} (nm)	λ_{em} (nm)	τ_{av} (ns)	φ (%)	λ_{exc} (nm)	λ_{em} (nm)	τ_{av}	φ (%)	λ_{exc} (nm)	λ_{em} (nm)	τ_{av} (μs)
1	445	511	4.91	3.85	430	627	2.26	4.08	430	^{I}627	2.83 ns	0.02	430	^{I}587,	^{I}3.6
										^{II}711	14.28 μs			^{II}688, 761	^{II}12 069
2	450	580	7.30	1.78	430	609	3.97	0.05	430	^{I}593	5.75 ns	1.40	470	707, 784	2590
										^{II}712	22.71 μs				

[a] τ_{av}: average lifetime of multiexponential fits of decay curves (see Figure S11 in the SI). φ: luminescence quantum yield.

LUMO+2 of **2** also have higher contributions of the 2-anthryl orbitals and are better energetically stabilized compared to those of **1**. Most importantly, the HOMO−LUMO energy gaps of compounds **1** and **2** become noticeably lower in comparison to the previously reported [ReCl(CO)$_3$(4′-Ar-terpy-κ^2N)] complex bearing the structural isomer 4′-(phenanthren-9-yl)-2,2′:6′,2″-terpyridine (Figure S11). In contrast to **1** and **2**, the HOMO of [ReCl(CO)$_3$(4′-Ar-terpy-κ^2N)] with 9-phenanthryl-terpy is distributed over the {ReCl(CO)$_3$} unit,[35] which also confirms a pivotal role of the molecular configuration of the appended aryl group. In contrast to linear anthracene, phenanthrene is nonlinear.

To examine the nature of electronic transitions of obtained complexes, time-dependent DFT (TD-DFT) calculations were performed using optimized structures of **1** and **2**. The calculated transitions along with the experimental spectra and natural transition orbitals for the lowest energy band of **1** and **2** are presented in Figure S12. For both complexes, the excitation $S_0 \rightarrow S_1$ can be assigned to the intraligand $\pi_{An} \rightarrow \pi^*_{terpy}$ and $\pi_{An} \rightarrow \pi^*_{An}/\pi^*_{terpy}$ transition for **1** and **2**, respectively. A twist of the 2-anthryl group, which is smaller than that of the 9-anthryl one, results in an increase in the oscillator strength of the $S_0 \rightarrow S_1$ transition for complex **2**, which correlates with the stronger absorptivity (ε) of **2** relative to that of **1** in the visible region. The character $\pi_{An} \rightarrow \pi^*_{terpy}/\pi^*_{An}$ can also be assigned to the $S_0 \rightarrow S_4$ transition, while the transitions $S_0 \rightarrow S_2$ and $S_0 \rightarrow S_3$ are of metal-to-ligand charge transfer (MLCT) nature (Table S4).

Excited-State Properties. Photoluminescence spectra of **1** and **2** are displayed in Figures 4 and S13−S19. Upon excitation into the red side of the lowest energy absorption, with λ_{exc} > 400 nm, the complexes in acetonitrile solution show broad and unstructured emission with maximum at 627 nm for **1** and 609 nm for **2** (Table 2). With reference to previously reported compounds [ReCl(CO)$_3$(4′-Ar-terpy-κ^2N)] incorporating 2,2′:6′,2″-terpyridines functionalized with 1-naphthyl, 2-naphthyl, and 9-phenanthryl groups, it can be derived that the emission of **1** and **2** in MeCN originates predominately from the ^{3}MLCT excited state (Figure S15). However, as shown in Figure S15, the emission bands of **1** and **2** are not completely superimposed over those for [ReCl(CO)$_3$(terpy-κ^2N)] and [ReCl(CO)$_3$(4′-Ar-terpy-κ^2N)] substituted with 1-naphthyl, 2-naphthyl, and 9-phenanthryl. Both maxima and onsets of the ^{3}MLCT emission of **1** and **2** are slightly blue-shifted relative to those previously reported, which may suggest some contribution of residual fluorescence due to any incomplete FRET from ^{1}IL to ^{1}MLCT, as reported previously for other bichromophoric systems.[31,32,75−77]

The contribution of the residual fluorescence becomes more noticeable when acetonitrile solutions of **1** and **2** are excited at the blue side of the lowest energy absorption. Irradiation with λ_{exc} = 355 nm predominately populates the ^{1}An state. Higher energy excitation results in dual fluorescence−phosphorescence emission for **1** and a significant hypsochromic shift of the structureless emission band for **2** (Figure 4 and Table S5). The replacement of acetonitrile by less polar chloroform induces noticeable changes in the photophysical properties of **1** and **2**. In this case, the emission of **1** excited at 355 nm and λ_{exc} > 410 nm appears at significantly shorter wavelengths (∼510 nm), and it can be assigned to ^{1}IL/^{1}ILCT fluorescence. The phosphorescence of the ^{3}MLCT origin of **1** may be effectively masked by brighter and faster fluorescence or even quenched by the lower-lying triplet state localized on the anthracene moiety, which is well recognized for bichromophoric systems with the anthracene unit.[32,41,78,79] The structureless emission band of **2** in $CHCl_3$ upon excitation λ_{exc} > 410 nm appears at ∼580 nm, which is bathochromically shifted by ∼135 nm compared to the free ligand in $CHCl_3$ (Figure S16). In addition, compared to the emission from the ^{3}MLCT excited state of **2** in MeCN, it is blue-shifted by ∼30 nm. This allows us to assume that the photophysics of **2** in $CHCl_3$ is determined by both the ^{1}IL/^{1}ILCT fluorescence and ^{3}MLCT phosphorescence. The presence of two components is clearly noticeable upon excitation of **2** in $CHCl_3$ at 410 nm (Figure S14). In DMSO, two emission bands are observed for both complexes **1** and **2** excited with λ_{exc} > 410 nm. The broad and weak component at higher energies falls in the range of ^{3}MLCT phosphorescence, while the structured emission at longer wavelengths (>680 nm) can be safely assigned to ^{3}An. Regarding excited-state lifetimes of ^{3}MLCT and ^{3}An, it can be assumed that they decay independently, there is no evidence of formation of the triplet-state equilibrium between the anthracene and {ReCl(CO)$_3$(terpy-κ^2N)} chromophores.

Higher energy excitation (λ_{exc} = 355 nm) of **1** in DMSO results in dual fluorescence−phosphorescence ligand-centered emission for **1**, while the emission spectrum of **2** still shows both ^{3}MLCT and ^{3}An components. However, compared to the spectra measured for lower energy excitation (λ_{exc} = 430 nm), the relative contribution of the ^{3}MLCT component is considerably enhanced. Most importantly, the anthracene-related room-temperature phosphorescence is rarely observed. For the first time, this was reported for Pt(II) bisacetylide complexes,[80] and its presence was rationalized by the enhanced effect of the heavy atom on anthracene.

To obtain further insights, the photoluminescence of [ReCl(CO)$_3$(4′-An-terpy-κ^2N)] was examined at a low temperature (77 K). The frozen-state emission spectra also revealed noticeable differences between **1** and **2** (Figure 4). For compound **1**, the emission spectrum at 77 K consists of two components: a broad and slightly structured emission band in the range of 480−670 nm, which overlaps with the phosphorescence of [ReCl(CO)$_3$(4′-Ar-terpy-κ^2N)] incorporating 2,2′:6′,2″-terpyridines functionalized with 1-naphthyl, 2-

https://doi.org/10.1021/acs.inorgchem.2c02160
Inorg. Chem. 2022, 61, 15070−15084

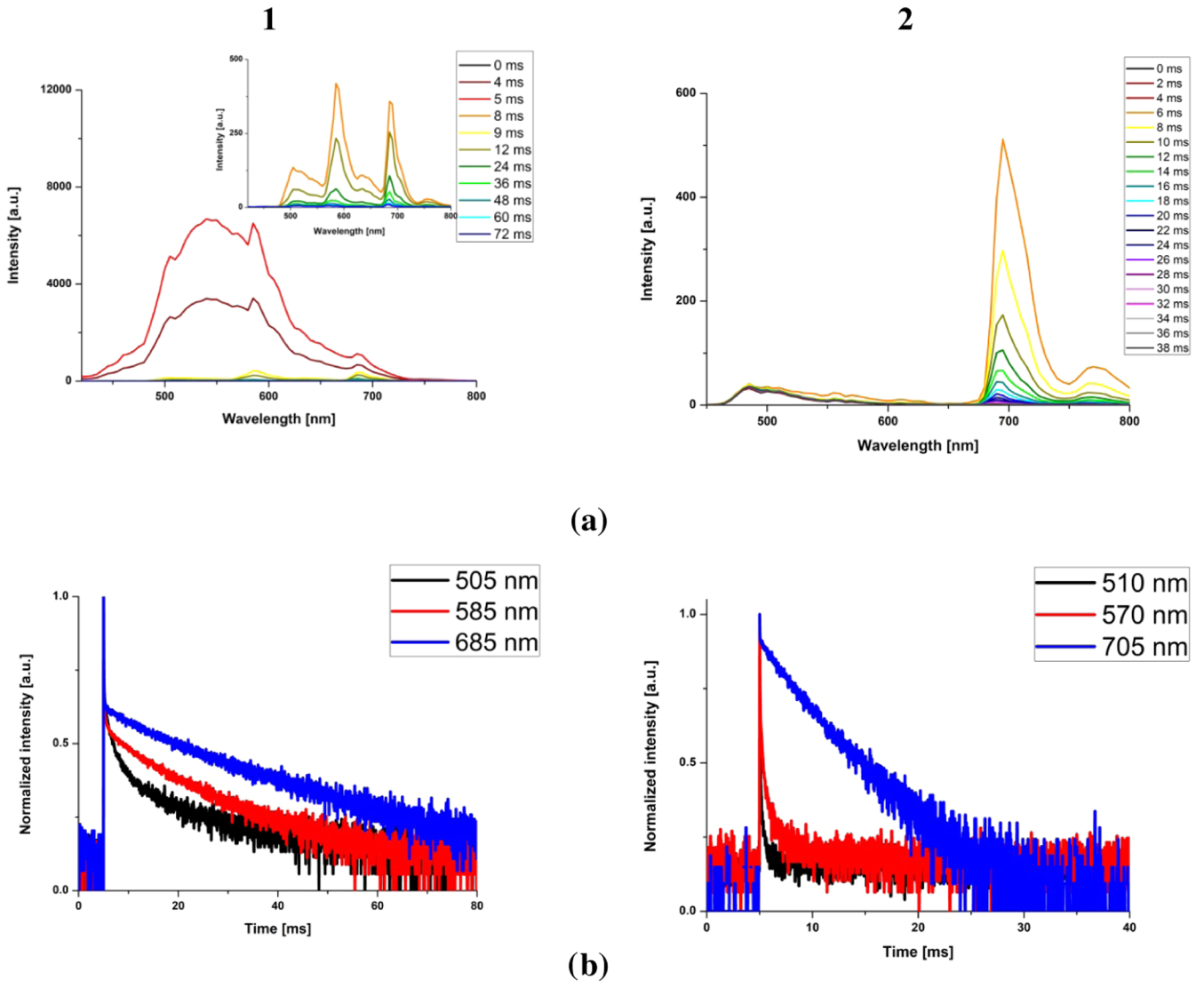

Figure 5. (a) Time-resolved emission spectra for **1** and **2** in the BuCN rigid matrix at 77 K (excitation wavelength: 405 nm and time window: 80 ms for **1**, and excitation wavelength: 405 nm and time window: 20 ms for **2**). (b) Decay curves for the maxima of emission bands observed in time-resolved emission spectra for **1** and **2** in the BuCN rigid matrix at 77 K.

naphthyl, and 9-phenanthrenyl groups (Figure S17), and a well-structured emission, which is superimposed over the phosphorescence of the free ligand and anthracene (Figure S18). A weak vibronic structure of the high-energy emission is assigned to a small contribution of $^3IL_{terpy}$, as reported for Re(I) carbonyl complexes with naphthyl- and phenanthrenyl-substituted terpyridine ligands.[35] In contrast, complex **2** shows mainly the emission band with a well-resolved vibronic structure in the range of 680−830 nm, originating from the $^3IL_{An}$ excited state. Relative to complex **1**, ^{3}An emission of **2** appears in a lower energy region, which can be rationalized by the negligible population of the ^{3}MLCT excited state, contrary to complex **1** (Figure 4).

The formation of the ^{3}MLCT state upon excitation of **2** was evidenced more clearly by time-resolved emission spectra (TRES) recorded at 77 K. As demonstrated in Figure 5, the ^{3}MLCT excited state of **2** almost immediately undergoes triplet−triplet energy transfer into ^{3}IL localized on the 2-anthryl-terpy ligand. Another striking difference between **1** and **2** concerns the relative contributions of the residual fluorescence, which is significantly larger for complex **1**.

The nature of the triplet excited state of [ReCl(CO)$_3$(4′-An-terpy-κ^2N)] was also investigated theoretically. In this regard, structures of **1** and **2** were optimized in their triplet states (T_1). The character of the lowest energy triplet excited state was assigned using the spin density surfaces generated from the lowest energy triplet state, and the phosphorescence energies were determined as the difference between the ground singlet and triplet states $\Delta E_{T_1-S_0}$.

As shown in Figure 6, the spin density surfaces of both **1** and **2** were distributed on the anthryl substituent and central pyridine of terpy, supporting the ^{3}An/^{3}(An-terpy) character of the lowest energy triplet state. Calculated phosphorescence energies, 905 nm for **1** and 886 nm for **2**, correlate well with the lowest energy shoulder of the structured triplet emission band of anthracene.[81]

Femtosecond Transient Absorption—The Nature of the Lowest Triplet-State and Excited-State Dynamics. The nature of the lowest triplet-state and excited-state dynamics of **1** and **2** was investigated by applying pump−probe transient absorption with femtosecond (fsTA) reso-

https://doi.org/10.1021/acs.inorgchem.2c02160
Inorg. Chem. 2022, 61, 15070−15084

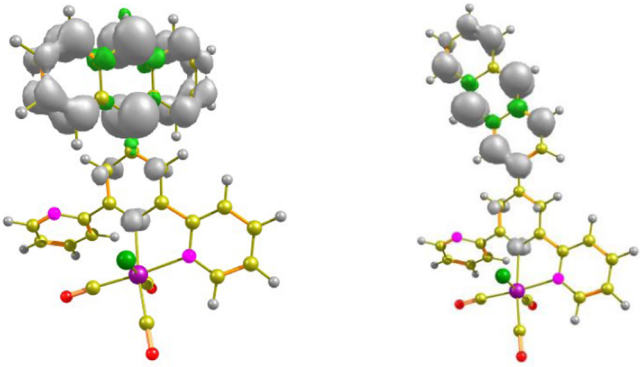

1 2

Figure 6. Spin density surface plots for **1** and **2**. Gray and green colors show regions of positive and negative spin density values, respectively (see also Table S6 in the SI).

lution. The measurements were performed for solutions of **1** and **2** in $CHCl_3$, MeCN, and DMSO upon excitation at 355 nm, as well as for **1** and **2** in $CHCl_3$ excited at 405 nm. After photoexcitations at 355 and 405 nm, both ^{1}An and ^{1}MLCT excited states are simultaneously populated, but a higher ^{1}An/^{1}MLCT population ratio is expected in the case of 355 nm excitation.

The results of fsTA experiments of complexes **1** and **2** together with global fitting analysis are summarized in Figures 7 and S21−S25.

The most intense excited-state absorption (ESA) of **1** in the range of 410−460 nm is a typical spectral feature corresponding to the $T_1 \rightarrow T_n$ transitions of anthracene.[46,47,65,78,82,83] It is the only signal at longer time delays, confirming that the lowest triplet state is localized on the anthracene chromophore. The ESA band starts rising almost immediately after photoexcitation and persists up to the end of the delay stage, as the ^{3}An lifetime is much longer than the maximum pump−probe time delay of the fsTA setup.[81] Regarding the spectral changes occurring at early time delays and previous reports on related systems,[37,47,84,85] we can assume that the final spectral component (^{3}An) of **1** is formed via two paths, ^{1}MLCT → ^{3}MLCT → ^{3}An and $S_1(^1An) \rightarrow T_2(^3An) \rightarrow T_1(^3An)$. The population of ^{3}An via two channels is clearly evidenced by the biphasic kinetics of growth displayed on time trace at 426 nm (see Figures 8, S23, and S24 showing time traces for selected wavelengths along with fitting curves obtained via global analysis). The ^{3}MLCT state is represented by ESA bands with maxima at ∼385 and ∼495 nm, in agreement with the results for the parent chromophore $[ReCl(CO)_3(terpy\text{-}\kappa^2N)]$[37] (Figure S25). The signal in the UV region is attributed to the absorption of polypyridine anion radicals, while ESA in the visible part corresponds to ligand-to-metal charge transfer (LMCT, $Cl/L^{\bullet-} \rightarrow Re$) transitions.[37,84,85] As reported by Yang,[47] spectral features attributable to $T_2(^3An) \rightarrow T_n(^3An)$ transitions are expected in the range of 500−600 nm, partly overlapping with the ESA of LMCT.

Time constants determined from global fit analysis are summarized in Table 3, and decay-associated spectra (DAS) are shown in column C in Figure 7. The ultrafast intersystem crossings, which occur in the time range shorter than the instrument response, are not included in Table 3. Besides the discarded ultrafast time constants, which can be safely assigned to the ultrafast ISC from the initially populated ^{1}MLCT to ^{3}MLCT,[37,84,85] four components are involved in the fsTA kinetics of **1**. The lifetimes t_2, t_3, and t_4 can be attributed to $S_1(^1An) \rightarrow T_2(^3An)$, $T_2(^3An) \rightarrow T_1(^3An)$, and ^{3}MLCT → ^{3}An processes, respectively. DAS_5 (with t_5 = inf) corresponds to the absorption spectrum of the fully relaxed lowest triplet state ^{3}An, which does not completely decay within the time scale of the measurement. The photophysical processes occurring upon photoexcitation of **1** are summarized in Scheme 2.

Excitation of **2** at both 355 and 405 nm results in an instant appearance of excited-state absorption (ESA) with the main peak at 460 nm and a minor one at 640 nm. Within about 2−5 ps, the intensity of the ESA at 460 nm increases and then starts to slowly decrease. The rise of the higher energy band is accompanied by a slight intensity decrease of the minor peak within this time scale. In analogy to **1**, the dominant ESA corresponding to the $T_1 \rightarrow T_n$ transitions of the anthracene unit does not completely decay within the time scale of the measurements, but a more planar geometry of 2-anthryl-terpy, and thus stronger electronic communication between the anthracene and $\{ReCl(CO)_3(terpy\text{-}\kappa^2N)\}$ chromophores, facilitates substantial population of the ^{3}An triplet state. Compared to **1**, however, $T_1 \rightarrow T_n$ absorption band shows noticeable red shift and broadening, which can be attributed to the stronger electronic coupling between An and terpy moieties in complex **2**.

For the best fitting of transient spectra kinetics of **2** upon excitation at 355 and 405 nm, three time constants were required (Table 3). Over the course of the first time constant (Table 3), the vibrationally hot ^{3}An excited state is formed. DAS_2 (corresponding to t_2), which is positive in the region corresponding to the fully relaxed lowest triplet state ^{3}An, reflects the vibrational relaxation of the lowest triplet state ^{3}An, comprising reorganization within the $[ReCl(CO)_3(4'\text{-}An\text{-}terpy\text{-}\kappa^2N)]$ bichromophore and interacting solvent molecules. DAS_3 with infinite lifetime corresponds to ground state recovery.

Abilities for $^1O_2$ Generation and Light Emission under the External Voltage. Since both complexes have long excited-state lifetimes (14 μs for **1** and 22 μs for **2** in DMSO), it can be anticipated that they are suitable for transferring the excited triplet-state energy to molecular oxygen, generating singlet oxygen. The ability of Re(I) complexes for photosensitized generation of singlet oxygen was examined by an indirect method with the use of diphenylisobenzofuran (DPBF), which is highly sensitive to $^1O_2$. Reacting with $^1O_2$, diphenylisobenzofuran forms endoperoxide, which spontaneously decomposes to 1,2-dibenzoylbenzene.[49,86−88] As shown in Figure 9, both complexes **1** and **2** exhibit singlet oxygen sensitizing ability. The insignificantly enhanced singlet oxygen sensitizing ability of **2** ($\Phi_{\Delta O_2}$ = 0.45) in relation to **1** ($\Phi_{\Delta O_2}$ = 0.42) correlates with its longer triplet excited-state lifetime in DMSO at room temperature (Table 2). For both complexes, the values of $\Phi_{\Delta O_2}$ are lower than that for anthracene (0.57) but ∼2 times greater than those for free ligands (0.21 for 9-anthryl-terpy and 0.23 for 2-anthryl-terpy; Figures S27 and S28). Relative to the efficient $[Ru(bipy)_3](PF_6)_2$ photosensitizer ($\Phi_{\Delta O_2}$: 0.66), however, the absorbance plots of DPBF in the presence of **1** and **2** display lower slopes, indicating their weaker abilities for $^1O_2$ generation.

https://doi.org/10.1021/acs.inorgchem.2c02160
Inorg. Chem. 2022, 61, 15070−15084

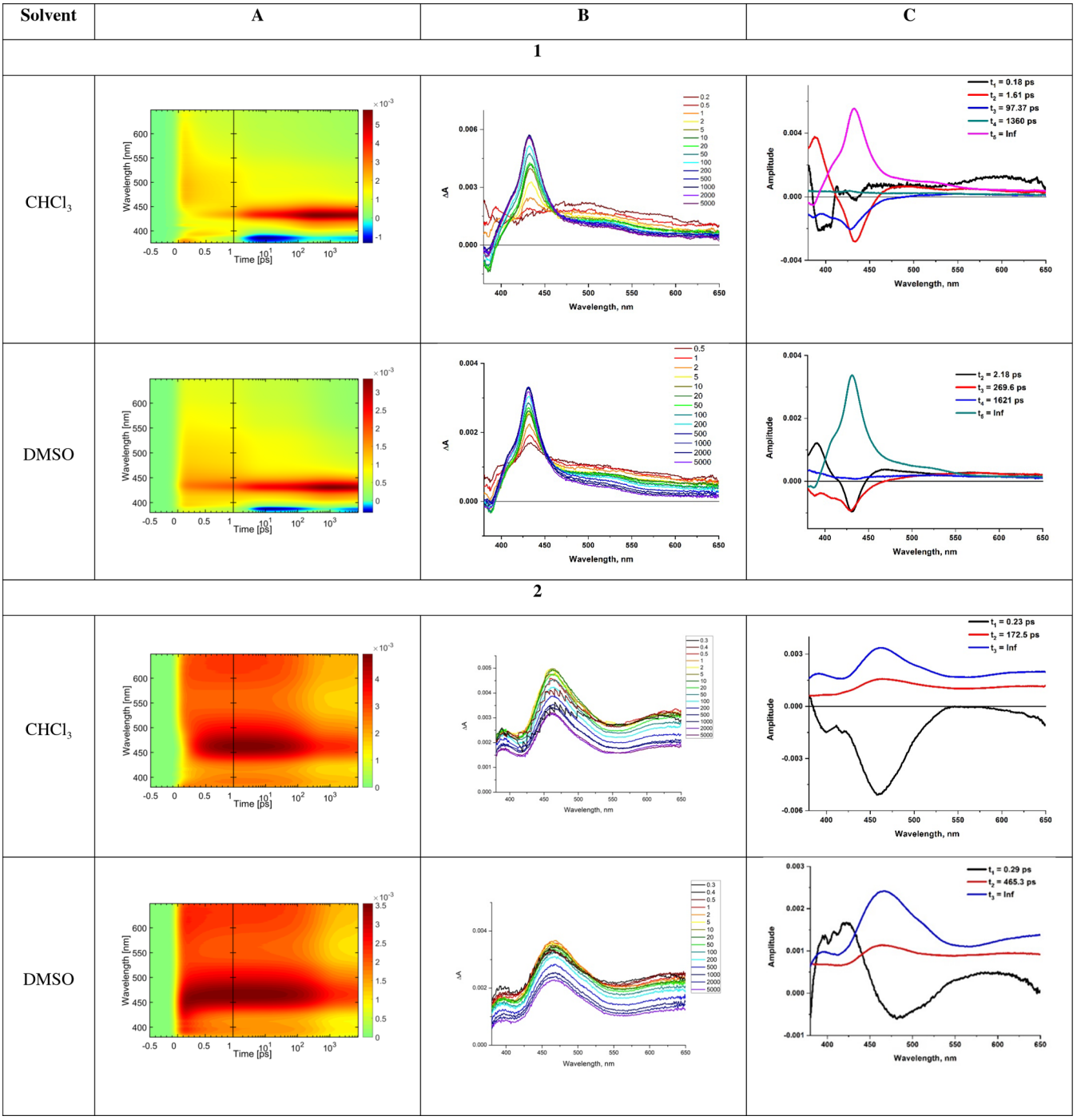

Figure 7. Summary of fsTA measurements for complexes **1** and **2** excited at 355 nm: fsTA 2D maps (A), TA spectra at selected time delays (B), and decay-associated spectra (DAS) (C) (see also Figures S21–S25).

To perform preliminary tests of [ReCl(CO)$_3$(An-terpy-κ^2N)] ability for light emission induced by voltage, two types of diodes with structures of ITO/PEDOT:PSS/complex/Al and ITO/PEDOT:PSS/PVK:PBD:complex/Al were fabricated. The matrix consisting of poly(9-vinylcarbazole) (PVK, 50 wt %) and (2-*tert*-butylphenyl-5-biphenyl-1,3,4-oxadiazole) (PBD, 50 wt %) was applied due to its effective charge carrier transport of ambipolar character. Moreover, diodes with such a guest–host configuration were also utilized in our previous investigations concerning Re(I) complexes.[35−37,67,68,70,71,73,82,89] As can be seen in Figure 3b, absorption of **1** and **2** partially overlaps with the emission spectrum of the host (matrix PVK:PBD), thus Förster energy transfer can be expected.[90] However, only the diode with complex **1** as an active layer showed weak emission with the maximum electroluminescence (EL) band (λ_{EL}) at 715 nm under 20 V, contrary to the device based on **2**, which was nonemissive. With reference to the discussion in the previous section, this weak emission can be assigned to anthracene phosphorescence.

In the case of diodes with guest–host structures, the emission was dependent on the applied voltage, and an increase of the applied voltage resulted in an increase in the

https://doi.org/10.1021/acs.inorgchem.2c02160
Inorg. Chem. 2022, 61, 15070−15084

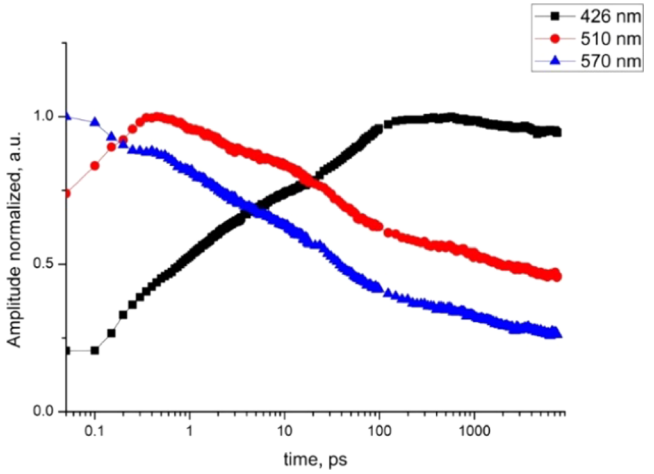

Figure 8. Time traces for representative wavelengths of 426 nm (maximum of $T_1(^3An) \rightarrow T_n(^3An)$ ESA), 510 nm (red edge of ^{3}LMCT ESA), and 570 nm (maximum of $T_2(^3An) \rightarrow T_n(^3An)$ ESA) for **1** in MeCN excited at 355 nm.

Table 3. Summary of the Time Constants (ps) from Global Fit Analysis

		405 nm	355 nm		
	t (ps)	$CHCl_3$	$CHCl_3$	MeCN	DMSO
1	t_1		0.18		
	t_2	1.53	1.61	1.93	2.18
	t_3	92.9	97.37	52.0	269.6
	t_4	1964	1360	1730	1621
	t_5	inf	inf	inf	inf
2	t_1	0.58	0.23	0.18	0.29
	t_2	168.8	172.5	105.1	465.3
	t_3	inf	inf	inf	inf

light emission. Nevertheless, rather high voltages were required to detect light emission (Figure 10).

Most importantly, the electroluminescence (EL) band of guest−host diodes covers a broad range from the visible (500 nm) to near-infrared region (750−900 nm), with λ_{EL} located at about 638 and 705 nm for **1** and 600, 705, and 778 for **2**. The addition of another component, emitting blue light from 400 to 500 nm, may yield a diode, which emits white light (WORED). The EL spectra are similar to the photoluminescence spectra of **1** and **2** registered in DMSO at RT and a rigid matrix at 77 K in BuCN (Figure 4). Regarding the complex content, the addition of 1 wt % gives the most intense emission. In turn, taking into consideration the anthryl linking mode, significantly more intense EL showed a device based on the complex with 2-anthryl substituent (**2**), which well correlates with the higher PL quantum yield of **2** in DMSO relative to **1**. To the best of our knowledge, such broad and structured emission, ranging to 900 nm with two or three maxima, was observed for the first time in diodes based on $[ReCl(CO)_3(4'\text{-Ar-terpy-}\kappa^2N)]$ compounds.[35−37,67,68,70,71,73,82,89] Indeed, diodes reported previously by our research group, Re(I) complexes based on 2,2′:6′,2″-terpyridines substituted with conjugated aryl groups such as 1-naphthyl, 2-naphthyl, 9-phenanthrenyl, and 1-pyrrenyl applied as guests in the PVK:PBD matrix (1, 2, and 15 wt %), exhibited λ_{EL} in ranges of 595−600, 595−610, 585−610, and 640−650 nm, respectively.[35] In addition, devices with molecularly dispersed Re(I) complexes bearing electron-donating amine units also showed emission in a significantly narrower spectral range.[72,91]

CONCLUSIONS

In summary, in-depth studies of the electrochemical and optical properties of two Re(I) complexes with 2,2′:6′,2″-terpyridines (terpy) substituted with the 9-anthryl (**1**) and 2-anthryl (**2**) confirmed a noticeable impact of the anthryl

Scheme 2. Representative Energy-Level Diagram along with Photophysical Processes Occurring upon Photoexcitation of 1[a]

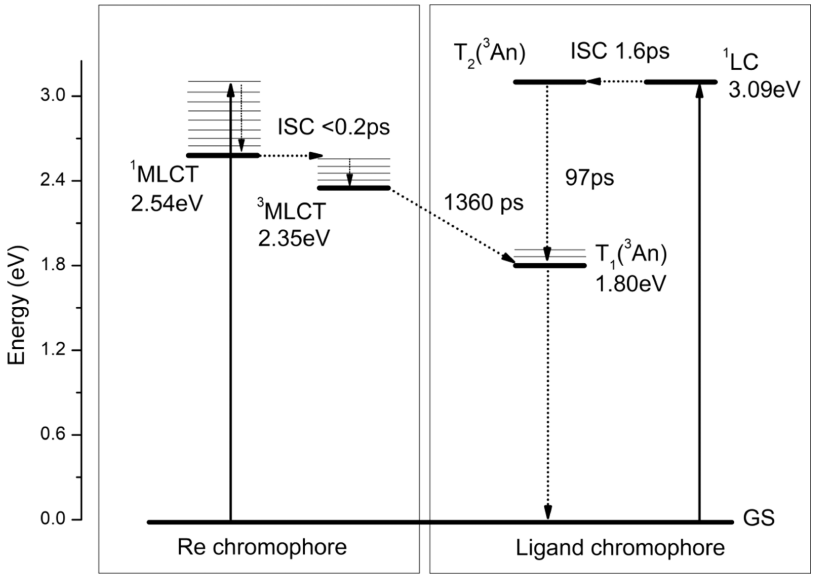

[a]The energies of ^{1}LC and ^{1}MLCT were estimated from onsets of the lowest energy absorption bands of the corresponding ligand and parental $[ReCl(CO)_3(terpy\text{-}\kappa^2N)]$ in $CHCl_3$, respectively, while ^{3}LC and ^{3}MLCT energies were obtained from onsets of 77 K phosphorescence of the organic ligand and the room-temperature emission of $[ReCl(CO)_3(terpy\text{-}\kappa^2N)]$ in $CHCl_3$, respectively.

https://doi.org/10.1021/acs.inorgchem.2c02160
Inorg. Chem. 2022, 61, 15070−15084

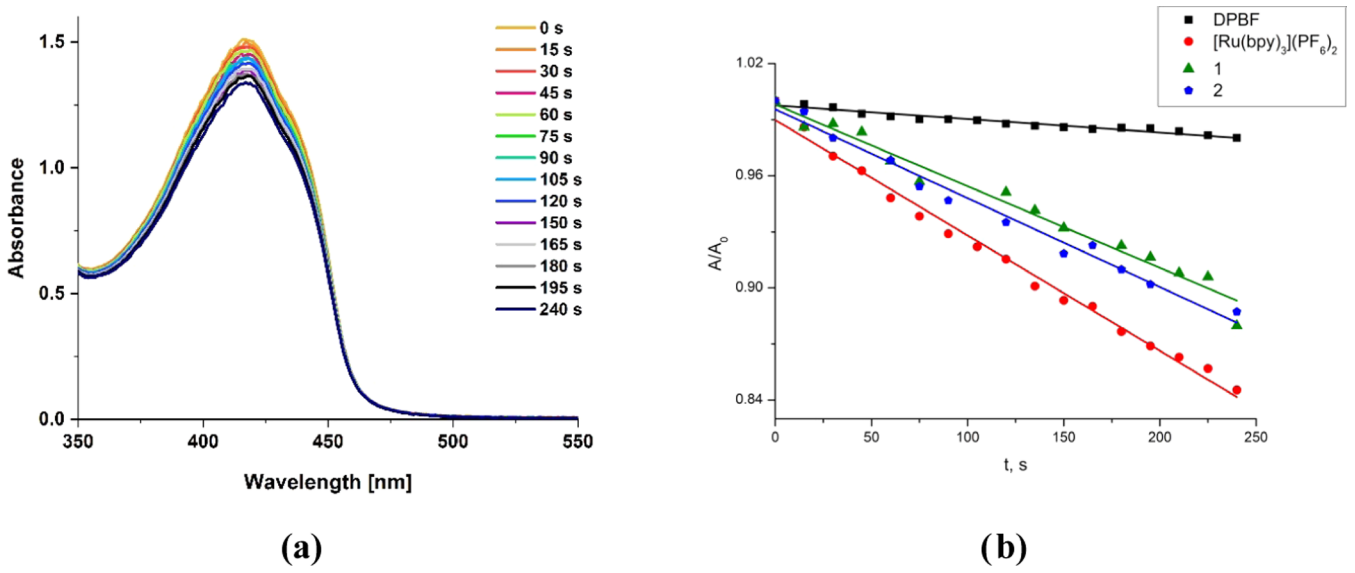

Figure 9. UV−vis absorption spectra of diphenylisobenzofuran (DPBF) in DMSO (c: 50 μM) treated with complex **1** (c: 50 μM) upon exposure to visible light at 420 nm recorded over 240 s (a) and relative changes in the absorbance of DPBF at 417 nm (A/A_0) with time (b).

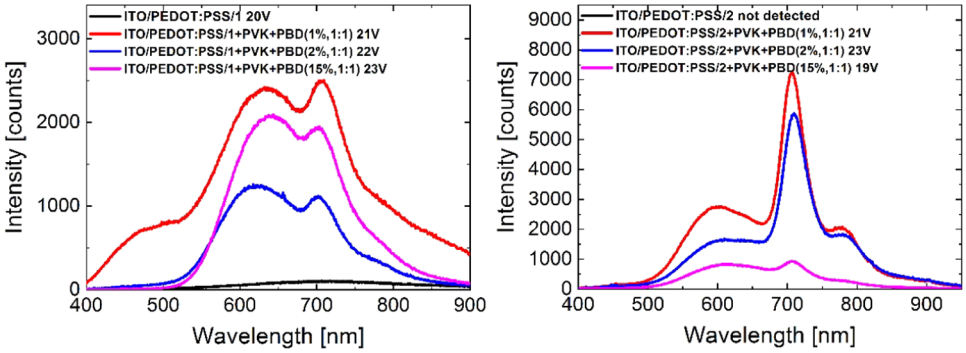

Figure 10. Electroluminescence spectra of diodes based on investigated Re(I) complexes with anthryl groups.

linking mode on the ground- and excited-state properties of resulting [ReCl(CO)$_3$(4′-An-terpy-κ^2N)]. As a result of the more extended overlapping orbitals of 2-anthryl and terpy moieties, the absorption band of **2** is shifted to lower energy and becomes slightly more intense compared to that of **1** with a clearly twisted geometry of 9-anthryl-terpy. The stronger electronic coupling between the anthracene and {ReCl(CO)$_3$(terpy-κ^2N)} chromophores also facilitates the population of the ^{3}An triplet state. Following the femtosecond transient absorption, the excitation of **2** results in an instant appearance of excited-state absorption (ESA) corresponding to the $T_1 \rightarrow T_n$ transitions of the anthracene unit, while the ^{3}An ESA of **1** is formed significantly slower, and its rise occurs via two independent channels. It is worth noticing that complexes **1** and **2** are rare examples that show anthracene-related room-temperature phosphorescence. However, although complexes **1** and **2** in DMSO excited with $\lambda_{ex} > 410$ nm show both ^{3}MLCT and ^{3}An emission bands, there was no evidence of formation of the equilibrium between the triplet states localized on anthracene and {ReCl(CO)$_3$(terpy-κ^2N)} chromophores. The excited states ^{3}MLCT and ^{3}An decay independently with different excited-state lifetimes. The presence of both ^{3}MLCT and ^{3}An emissions was also observed in the electroluminescence band of guest−host diodes based on investigated Re(I) complexes. Having long excited-state lifetimes in DMSO, the examined carbonyls were found to be suitable for transferring the excited triplet-state energy to molecular oxygen, generating singlet oxygen. We strongly believe that reported findings will be useful for understanding and controlling the excited-state nature of transition metal complexes and thus designing photoluminescent materials with predefined photophysical properties.

■ ASSOCIATED CONTENT

Supporting Information

The Supporting Information is available free of charge at https://pubs.acs.org/doi/10.1021/acs.inorgchem.2c02160.

NMR (^{1}H, ^{13}C, and 2D); IR and HRMS spectra; stability and photostability; UV−vis spectra; DFT and TD-DFT calculations; steady-state and time-resolved emission spectra; spin density surface plots; femtosecond transient absorption spectra; and global fitting results (PDF)

■ AUTHOR INFORMATION

Corresponding Author

Barbara Machura − *Institute of Chemistry, University of Silesia, 40-006 Katowice, Poland;* orcid.org/0000-0001-7688-6491; Phone: +48 32 3591718; Email: barbara.machura@us.edu.pl

https://doi.org/10.1021/acs.inorgchem.2c02160
Inorg. Chem. 2022, 61, 15070−15084

Authors

Magdalena Małecka − *Institute of Chemistry, University of Silesia, 40-006 Katowice, Poland*

Agata Szlapa-Kula − *Institute of Chemistry, University of Silesia, 40-006 Katowice, Poland;* orcid.org/0000-0001-6539-5419

Anna M. Maroń − *Institute of Chemistry, University of Silesia, 40-006 Katowice, Poland;* orcid.org/0000-0001-8245-5532

Przemyslaw Ledwon − *Department of Physical Chemistry and Technology of Polymers, Silesian University of Technology, 44-100 Gliwice, Poland;* orcid.org/0000-0001-6769-8739

Mariola Siwy − *Centre of Polymer and Carbon Materials, Polish Academy of Sciences, 41-819 Zabrze, Poland*

Ewa Schab-Balcerzak − *Institute of Chemistry, University of Silesia, 40-006 Katowice, Poland; Centre of Polymer and Carbon Materials, Polish Academy of Sciences, 41-819 Zabrze, Poland;* orcid.org/0000-0002-7219-8664

Karolina Sulowska − *Nanophotonics Group, Institute of Physics, Faculty of Physics, Astronomy and Informatics, Nicolaus Copernicus University, 87-100 Torun, Poland*

Sebastian Maćkowski − *Nanophotonics Group, Institute of Physics, Faculty of Physics, Astronomy and Informatics, Nicolaus Copernicus University, 87-100 Torun, Poland;* orcid.org/0000-0003-1560-6315

Karol Erfurt − *Department of Chemical Organic Technology and Petrochemistry, Silesian University of Technology, 44-100 Gliwice, Poland*

Complete contact information is available at: https://pubs.acs.org/10.1021/acs.inorgchem.2c02160

Author Contributions

M.M. and A.M.M.: formal analysis, investigation, methodology, data curation, and visualization; A.S.-K.: investigation, methodology, formal analysis, resources, visualization, and data curation; P.L., M.S., K.S., and K.E.: investigation; S.M.: investigation and validation; E.S.-B.: formal analysis, methodology, resources, and writing—original draft; B.M.: conceptualization, formal analysis, funding acquisition, methodology, project administration, resources, supervision, validation, writing—original draft, and writing—review and editing.

Notes

The authors declare no competing financial interest.

■ ACKNOWLEDGMENTS

The research was cofinanced by the National Science Centre of Poland grant no. DEC-2017/25/B/ST5/01611 (B.M.) and funds granted under the Research Excellence Initiative of the University of Silesia in Katowice. The calculations were carried out at Wroclaw Centre for Networking and Supercomputing (http://www.wcss.wroc.pl). M.M. thanks to PIK—Programme for new interdisciplinary elements of education at the doctoral level for a field of chemistry, POWR.03.02.00-00-I010/17.

■ REFERENCES

(1) Wrighton, M.; Morse, D. L. Nature of the Lowest Excited State in Tricarbonylchloro-1,10-Phenanthrolinerhenium(I) and Related Complexes. *J. Am. Chem. Soc.* **1974**, *96*, 998−1003.

(2) Stufkens, D. J.; Vlček, A. Ligand-Dependent Excited State Behaviour of Re(I) and Ru(II) Carbonyl−Diimine Complexes. *Coord. Chem. Rev.* **1998**, *177*, 127−179.

(3) Striplin, D. R.; Crosby, G. A. Photophysical Investigations of Rhenium(I)Cl(CO)3(Phenanthroline) Complexes. *Coord. Chem. Rev.* **2001**, *211*, 163−175.

(4) Vlček, A.; Záliš, S. Modeling of Charge-Transfer Transitions and Excited States in D6 Transition Metal Complexes by DFT Techniques. *Coord. Chem. Rev.* **2007**, *251*, 258−287.

(5) Coleman, A.; Brennan, C.; Vos, J. G.; Pryce, M. T. Photophysical Properties and Applications of Re(I) and Re(I)−Ru(II) Carbonyl Polypyridyl Complexes. *Coord. Chem. Rev.* **2008**, *252*, 2585−2595.

(6) Kumar, A.; Sun, S.-S.; Lees, A. J. Photophysics and Photochemistry of Organometallic Rhenium Diimine Complexes. In *Photophysics of Organometallics*; Lees, A. J., Ed.; Springer: Berlin, Heidelberg, 2010; pp 37−71.

(7) Ko, C.-C.; Cheung, A. W.-Y.; Lo, L. T.-L.; Siu, J. W.-K.; Ng, C.-O.; Yiu, S.-M. Syntheses and Photophysical Studies of New Classes of Luminescent Isocyano Rhenium(I) Diimine Complexes. *Coord. Chem. Rev.* **2012**, *256*, 1546−1555.

(8) Daniel, C. Photochemistry and Photophysics of Transition Metal Complexes: Quantum Chemistry. *Coord. Chem. Rev.* **2015**, *282*−*283*, 19−32.

(9) Lee, L. C.-C.; Leung, K.-K.; Lo, K. K.-W. Recent Development of Luminescent Rhenium(I) Tricarbonyl Polypyridine Complexes as Cellular Imaging Reagents, Anticancer Drugs, and Antibacterial Agents. *Dalton Trans.* **2017**, *46*, 16357−16380.

(10) Yang, J.; Zhao, J.-X.; Cao, Q.; Hao, L.; Zhou, D.; Gan, Z.; Ji, L.-N.; Mao, Z.-W. Simultaneously Inducing and Tracking Cancer Cell Metabolism Repression by Mitochondria-Immobilized Rhenium(I) Complex. *ACS Appl. Mater. Interfaces* **2017**, *9*, 13900−13912.

(11) Hostachy, S.; Policar, C.; Delsuc, N. Re(I) Carbonyl Complexes: Multimodal Platforms for Inorganic Chemical Biology. *Coord. Chem. Rev.* **2017**, *351*, 172−188.

(12) Bauer, E. B.; Haase, A. A.; Reich, R. M.; Crans, D. C.; Kühn, F. E. Organometallic and Coordination Rhenium Compounds and Their Potential in Cancer Therapy. *Coord. Chem. Rev.* **2019**, *393*, 79−117.

(13) Zhang, Q.; Wong, K. M.-C. Photophysical, Ion-Sensing and Biological Properties of Rhodamine-Containing Transition Metal Complexes. *Coord. Chem. Rev.* **2020**, *416*, No. 213336.

(14) Liew, H. S.; Mai, C.-W.; Zulkefeli, M.; Madheswaran, T.; Kiew, L. V.; Delsuc, N.; Low, M. L. Recent Emergence of Rhenium(I) Tricarbonyl Complexes as Photosensitisers for Cancer Therapy. *Molecules* **2020**, *25*, No. 4176.

(15) Pan, Z.-Y.; Cai, D.-H.; He, L. Dinuclear Phosphorescent Rhenium(I) Complexes as Potential Anticancer and Photodynamic Therapy Agents. *Dalton Trans.* **2020**, *49*, 11583−11590.

(16) Marker, S. C.; King, A. P.; Granja, S.; Vaughn, B.; Woods, J. J.; Boros, E.; Wilson, J. J. Exploring the In Vivo and In Vitro Anticancer Activity of Rhenium Isonitrile Complexes. *Inorg. Chem.* **2020**, *59*, 10285−10303.

(17) Karges, J.; Kalaj, M.; Gembicky, M.; Cohen, S. M. ReI Tricarbonyl Complexes as Coordinate Covalent Inhibitors for the SARS-CoV-2 Main Cysteine Protease. *Angew. Chem.* **2021**, *133*, 10811−10818.

(18) Gong, J.; Zhang, X. Coordination-Based Circularly Polarized Luminescence Emitters: Design Strategy and Application in Sensing. *Coord. Chem. Rev.* **2022**, *453*, No. 214329.

(19) Evans, R. C.; Douglas, P.; Winscom, C. J. Coordination Complexes Exhibiting Room-Temperature Phosphorescence: Evaluation of Their Suitability as Triplet Emitters in Organic Light Emitting Diodes. *Coord. Chem. Rev.* **2006**, *250*, 2093−2126.

(20) Werrett, M. V.; Huff, G. S.; Muzzioli, S.; Fiorini, V.; Zacchini, S.; Skelton, B. W.; Maggiore, A.; Malicka, J. M.; Cocchi, M.; Gordon, K. C.; Stagni, S.; Massi, M. Methylated Re(I) Tetrazolato Complexes: Photophysical Properties and Light Emitting Devices. *Dalton Trans.* **2015**, *44*, 8379−8393.

(21) Zhao, G.-W.; Zhao, J.-H.; Hu, Y.-X.; Zhang, D.-Y.; Li, X. Recent Advances of Neutral Rhenium(I) Tricarbonyl Complexes for Application in Organic Light-Emitting Diodes. *Synth. Met.* **2016**, *212*, 131−141.

(22) Hu, Y.-X.; Zhao, G.-W.; Dong, Y.; Lü, Y.-L.; Li, X.; Zhang, D.-Y. New Rhenium(I) Complex with Thiadiazole-Annelated 1,10-Phenanthroline for Highly Efficient Phosphorescent OLEDs. *Dyes Pigm.* **2017**, *137*, 569−575.
(23) Li, X.; Zhao, G.-W.; Hu, Y.-X.; Zhao, J.-H.; Dong, Y.; Zhou, L.; Lv, Y.-L.; Chi, H.-J.; Su, Z. Rational Design and Characterization of Novel Phosphorescent Rhenium(I) Complexes for Extremely High-Efficiency Organic Light-Emitting Diodes. *J. Mater. Chem. C* **2017**, *5*, 7629−7636.
(24) Takeda, H.; Ishitani, O. Development of Efficient Photocatalytic Systems for CO2 Reduction Using Mononuclear and Multinuclear Metal Complexes Based on Mechanistic Studies. *Coord. Chem. Rev.* **2010**, *254*, 346−354.
(25) Grills, D. C.; Fujita, E. New Directions for the Photocatalytic Reduction of CO2: Supramolecular, ScCO2 or Biphasic Ionic Liquid−scCO2 Systems. *J. Phys. Chem. Lett.* **2010**, *1*, 2709−2718.
(26) Doherty, M. D.; Grills, D. C.; Muckerman, J. T.; Polyansky, D. E.; Fujita, E. Toward More Efficient Photochemical CO2 Reduction: Use of ScCO2 or Photogenerated Hydrides. *Coord. Chem. Rev.* **2010**, *254*, 2472−2482.
(27) Zarkadoulas, A.; Koutsouri, E.; Kefalidi, C.; Mitsopoulou, C. A. Rhenium Complexes in Homogeneous Hydrogen Evolution. *Coord. Chem. Rev.* **2015**, *304*−*305*, 55−72.
(28) Nganga, J. K.; Samanamu, C. R.; Tanski, J. M.; Pacheco, C.; Saucedo, C.; Batista, V. S.; Grice, K. A.; Ertem, M. Z.; Angeles-Boza, A. M. Electrochemical Reduction of CO2 Catalyzed by Re(Pyridine-Oxazoline)(CO)3Cl Complexes. *Inorg. Chem.* **2017**, *56*, 3214−3226.
(29) Nandal, N.; Jain, S. L. A Review on Progress and Perspective of Molecular Catalysis in Photoelectrochemical Reduction of CO2. *Coord. Chem. Rev.* **2022**, *451*, No. 214271.
(30) Yarnell, J. E.; Deaton, J. C.; McCusker, C. E.; Castellano, F. N. Bidirectional "Ping-Pong" Energy Transfer and 3000-Fold Lifetime Enhancement in a Re(I) Charge Transfer Complex. *Inorg. Chem.* **2011**, *50*, 7820−7830.
(31) Yarnell, J. E.; Wells, K. A.; Palmer, J. R.; Breaux, J. M.; Castellano, F. N. Excited-State Triplet Equilibria in a Series of Re(I)-Naphthalimide Bichromophores. *J. Phys. Chem. B* **2019**, *123*, 7611−7627.
(32) Wells, K. A.; Yarnell, J. E.; Palmer, J. R.; Lee, T. S.; Papa, C. M.; Castellano, F. N. Energy Migration Processes in Re(I) MLCT Complexes Featuring a Chromophoric Ancillary Ligand. *Inorg. Chem.* **2020**, *59*, 8259−8271.
(33) Shillito, G. E.; Hall, T. B. J.; Preston, D.; Traber, P.; Wu, L.; Reynolds, K. E. A.; Horvath, R.; Sun, X. Z.; Lucas, N. T.; Crowley, J. D.; George, M. W.; Kupfer, S.; Gordon, K. C. Dramatic Alteration of 3ILCT Lifetimes Using Ancillary Ligands in [Re(L)(CO)3(Phen-TPA)]N+ Complexes: An Integrated Spectroscopic and Theoretical Study. *J. Am. Chem. Soc.* **2018**, *140*, 4534−4542.
(34) Fernández-Terán, R.; Sévery, L. Living Long and Prosperous: Productive Intraligand Charge-Transfer States from a Rhenium(I) Terpyridine Photosensitizer with Enhanced Light Absorption. *Inorg. Chem.* **2021**, *60*, 1334−1343.
(35) Szlapa-Kula, A.; Małecka, M.; Maroń, A. M.; Janeczek, H.; Siwy, M.; Schab-Balcerzak, E.; Szalkowski, M.; Maćkowski, S.; Pedzinski, T.; Erfurt, K.; Machura, B. In-Depth Studies of Ground- and Excited-State Properties of Re(I) Carbonyl Complexes Bearing 2,2′:6′,2″-Terpyridine and 2,6-Bis(Pyrazin-2-Yl)Pyridine Coupled with π-Conjugated Aryl Chromophores. *Inorg. Chem.* **2021**, *60*, 18726−18738.
(36) Maroń, A. M.; Szlapa-Kula, A.; Matussek, M.; Kruszynski, R.; Siwy, M.; Janeczek, H.; Grzelak, J.; Maćkowski, S.; Schab-Balcerzak, E.; Machura, B. Photoluminescence Enhancement of Re(i) Carbonyl Complexes Bearing D−A and D−π−A Ligands. *Dalton Trans.* **2020**, *49*, 4441−4453.
(37) Choroba, K.; Kotowicz, S.; Maroń, A.; Świtlicka, A.; Szłapa-Kula, A.; Siwy, M.; Grzelak, J.; Sulowska, K.; Maćkowski, S.; Schab-Balcerzak, E.; Machura, B. Ground- and Excited-State Properties of Re(I) Carbonyl Complexes—Effect of Triimine Ligand Core and Appended Heteroaromatic Groups. *Dyes Pigm.* **2021**, *192*, No. 109472.
(38) Wang, X.-y.; Del Guerzo, A.; Schmehl, R. H. Photophysical Behavior of Transition Metal Complexes Having Interacting Ligand Localized and Metal-to-Ligand Charge Transfer States. *J. Photochem. Photobiol., C* **2004**, *5*, 55−77.
(39) McClenaghan, N. D.; Leydet, Y.; Maubert, B.; Indelli, M. T.; Campagna, S. Excited-State Equilibration: A Process Leading to Long-Lived Metal-to-Ligand Charge Transfer Luminescence in Supramolecular Systems. *Coord. Chem. Rev.* **2005**, *249*, 1336−1350.
(40) Wang, J.; Fang, Y.-Q.; Bourget-Merle, L.; Polson, M. I. J.; Hanan, G. S.; Juris, A.; Loiseau, F.; Campagna, S. The Multichromophore Approach: Prolonged Room-Temperature Luminescence Lifetimes in RuII Complexes Based on Tridentate Polypyridine Ligands. *Chem.—Eur. J.* **2006**, *12*, 8539−8548.
(41) Liu, Y.-J.; Wang, K.-Z. Visible-Light-Excited Singlet-Oxygen Luminescence Probe Based on Re(CO)3Cl(Aeip). *Eur. J. Inorg. Chem.* **2008**, *2008*, 5214−5219.
(42) Ragone, F.; Saavedra, H. H. M.; Gara, P. M. D.; Ruiz, G. T.; Wolcan, E. Photosensitized Generation of Singlet Oxygen from Re(I) Complexes: A Photophysical Study Using LIOAS and Luminescence Techniques. *J. Phys. Chem. A* **2013**, *117*, 4428−4435.
(43) Gu, J.; Yan, Y.; Helbig, B. J.; Huang, Z.; Lian, T.; Schmehl, R. H. The Influence of Ligand Localized Excited States on the Photophysics of Second Row and Third Row Transition Metal Terpyridyl Complexes: Recent Examples and a Case Study. *Coord. Chem. Rev.* **2015**, *282*−*283*, 100−109.
(44) Kisel, K. S.; Eskelinen, T.; Zafar, W.; Solomatina, A. I.; Hirva, P.; Grachova, E. V.; Tunik, S. P.; Koshevoy, I. O. Chromophore-Functionalized Phenanthro-Diimine Ligands and Their Re(I) Complexes. *Inorg. Chem.* **2018**, *57*, 6349−6361.
(45) Zhang, X.; Hou, Y.; Xiao, X.; Chen, X.; Hu, M.; Geng, X.; Wang, Z.; Zhao, J. Recent Development of the Transition Metal Complexes Showing Strong Absorption of Visible Light and Long-Lived Triplet Excited State: From Molecular Structure Design to Photophysical Properties and Applications. *Coord. Chem. Rev.* **2020**, *417*, No. 213371.
(46) Hou, Y.; Biskup, T.; Rein, S.; Wang, Z.; Bussotti, L.; Russo, N.; Foggi, P.; Zhao, J.; Di Donato, M.; Mazzone, G.; Weber, S. Spin−Orbit Charge Recombination Intersystem Crossing in Phenothiazine−Anthracene Compact Dyads: Effect of Molecular Conformation on Electronic Coupling, Electronic Transitions, and Electron Spin Polarizations of the Triplet States. *J. Phys. Chem. C* **2018**, *122*, 27850−27865.
(47) Yang, W.; Zhao, J.; Tang, G.; Li, X.; Gurzadyan, G. G. Direct Observation of Long-Lived Upper Excited Triplet States and Intersystem Crossing in Anthracene-Containing PtII Complexes. *J. Phys. Chem. Lett.* **2019**, *10*, 7767−7773.
(48) Szlapa-Kula, A.; Małecka, M.; Machura, B. Insight into Structure-Property Relationships of Aryl-Substituted 2,2′:6′,2″-Terpyridines. *Dyes Pigm.* **2020**, *180*, No. 108480.
(49) Yuan, Z.; He, J.; Mahmood, Z.; Xing, L.; Ji, S.; Huo, Y.; Zhang, H.-L. Deciphering the Ligand's Geometric Effect on the Photophysical Properties of Osmium Complex and Its Application in Triplet-Triplet Annihilation Upconversion. *Dyes Pigm.* **2022**, *199*, No. 110049.
(50) Lutkus, L. V.; Rickenbach, S. S.; McCormick, T. M. Singlet Oxygen Quantum Yields Determined by Oxygen Consumption. *J. Photochem. Photobiol., A* **2019**, *378*, 131−135.
(51) van Wilderen, L. J. G. W.; Lincoln, C. N.; van Thor, J. J. Modelling Multi-Pulse Population Dynamics from Ultrafast Spectroscopy. *PLoS One* **2011**, *6*, No. e17373.
(52) Slavov, C.; Hartmann, H.; Wachtveitl, J. Implementation and Evaluation of Data Analysis Strategies for Time-Resolved Optical Spectroscopy. *Anal. Chem.* **2015**, *87*, 2328−2336.
(53) Frisch, M. J.; Trucks, G. W.; Schlegel, H. B.; Scuseria, G. E.; Robb, M. A.; Cheeseman, J. R.; Scalmani, G.; Barone, V.; Petersson, G. A.; Nakatsuji, H.; Li, X.; Caricato, M.; Marenich, A. V.; Bloino, J.; Janesko, B. G.; Gomperts, R.; Mennucci, B.; Hratchian, H. P.; Ortiz, J.

https://doi.org/10.1021/acs.inorgchem.2c02160
Inorg. Chem. 2022, 61, 15070−15084

V.; Izmaylov, A. F.; Sonnenberg, J. L.; Williams-Young, D.; Ding, F.; Lipparini, F.; Egidi, F.; Goings, J.; Peng, B.; Petrone, A.; Henderson, T.; Ranasinghe, D.; Zakrzewski, V. G.; Gao, J.; Rega, N.; Zheng, G.; Liang, W.; Hada, M.; Ehara, M.; Toyota, K.; Fukuda, R.; Hasegawa, J.; Ishida, M.; Nakajima, T.; Honda, Y.; Kitao, O.; Nakai, H.; Vreven, T.; Throssell, K.; Montgomery, J. A., Jr.; Peralta, J. E.; Ogliaro, F.; Bearpark, M. J.; Heyd, J. J.; Brothers, E. N.; Kudin, K. N.; Staroverov, V. N.; Keith, T. A.; Kobayashi, R.; Normand, J.; Raghavachari, K.; Rendell, A. P.; Burant, J. C.; Iyengar, S. S.; Tomasi, J.; Cossi, M.; Millam, J. M.; Klene, M.; Adamo, C.; Cammi, R.; Ochterski, J. W.; Martin, R. L.; Morokuma, K.; Farkas, O.; Foresman, J. B.; Fox, D. J. *Gaussian 16*, revision C.01; Gaussian, Inc.: Wallingford, CT, 2016.

(54) Perdew, J. P.; Burke, K.; Ernzerhof, M. Generalized Gradient Approximation Made Simple. *Phys. Rev. Lett.* **1996**, *77*, 3865−3868.

(55) Adamo, C.; Barone, V. Toward Reliable Density Functional Methods without Adjustable Parameters: The PBE0 Model. *J. Chem. Phys.* **1999**, *110*, 6158−6170.

(56) Weigend, F.; Ahlrichs, R. Balanced Basis Sets of Split Valence, Triple Zeta Valence and Quadruple Zeta Valence Quality for H to Rn: Design and Assessment of Accuracy. *Phys. Chem. Chem. Phys.* **2005**, *7*, 3297−3305.

(57) Rappoport, D.; Furche, F. Property-Optimized Gaussian Basis Sets for Molecular Response Calculations. *J. Chem. Phys.* **2010**, *133*, No. 134105.

(58) Cancès, E.; Mennucci, B.; Tomasi, J. A New Integral Equation Formalism for the Polarizable Continuum Model: Theoretical Background and Applications to Isotropic and Anisotropic Dielectrics. *J. Chem. Phys.* **1997**, *107*, 3032−3041.

(59) Cossi, M.; Barone, V.; Mennucci, B.; Tomasi, J. Ab Initio Study of Ionic Solutions by a Polarizable Continuum Dielectric Model. *Chem. Phys. Lett.* **1998**, *286*, 253−260.

(60) Witkowska, E.; Orwat, B.; Oh, M. J.; Wiosna-Salyga, G.; Glowacki, I.; Kownacki, I.; Jankowska, K.; Kubicki, M.; Gierczyk, B.; Dutkiewicz, M.; Grzelak, I.; Hoffmann, M.; Nawrocik, J.; Krajewski, G.; Ulanski, J.; Ledwon, P.; Lapkowski, M. Effect of β-Ketoiminato Ancillary Ligand Modification on Emissive Properties of New Iridium Complexes. *Inorg. Chem.* **2019**, *58*, 15671−15686.

(61) Ou, Y.-P.; Jiang, C.; Wu, D.; Xia, J.; Yin, J.; Jin, S.; Yu, G.-A.; Liu, S. H. Synthesis, Characterization, and Properties of Anthracene-Bridged Bimetallic Ruthenium Vinyl Complexes [RuCl(CO)(PMe3)-3]2(μ-CH═CH-Anthracene-CH═CH. *Organometallics* **2011**, *30*, 5763−5770.

(62) Garino, C.; Ghiani, S.; Gobetto, R.; Nervi, C.; Salassa, L.; Croce, G.; Milanesio, M.; Rosenberg, E.; Ross, J. B. A. Tricarbonylchlororhenium(I) Carboxaldimine Derivatives: Synthesis, Structure, and NMR Characterization of Z and E Isomers. *Eur. J. Inorg. Chem.* **2006**, *2006*, 2885−2893.

(63) Natarajan, P.; Schmittel, M. ON-OFF Luminescence Signaling of Hybrid Organic−Inorganic Switches. *Inorg. Chem.* **2013**, *52*, 8579−8590.

(64) Choroba, K.; Kula, S.; Maroń, A.; Machura, B.; Małecki, J.; Szłapa-Kula, A.; Siwy, M.; Grzelak, J.; Maćkowski, S.; Schab-Balcerzak, E. Aryl Substituted 2,6-Di(Thiazol-2-Yl)Pyridines −Excited-State Characterization and Potential for OLEDs. *Dyes Pigm.* **2019**, *169*, 89−104.

(65) Chen, K.; Kurganskii, I. V.; Zhang, X.; Elmali, A.; Zhao, J.; Karatay, A.; Fedin, M. V. Intersystem Crossing and Electron Spin Selectivity in Anthracene-Naphthalimide Compact Electron Donor-Acceptor Dyads Showing Different Geometry and Electronic Coupling Magnitudes. *Chem.—Eur. J.* **2021**, *27*, 7572−7587.

(66) Juris, A.; Campagna, S.; Bidd, I.; Lehn, J. M.; Ziessel, R. Synthesis and Photophysical and Electrochemical Properties of New Halotricarbonyl(Polypyridine)Rhenium(I) Complexes. *Inorg. Chem.* **1988**, *27*, 4007−4011.

(67) Klemens, T.; Świtlicka-Olszewska, A.; Machura, B.; Grucela, M.; Janeczek, H.; Schab-Balcerzak, E.; Szlapa, A.; Kula, S.; Krompiec, S.; Smolarek, K.; Kowalska, D.; Mackowski, S.; Erfurt, K.; Lodowski, P. Synthesis, Photophysical Properties and Application in Organic Light Emitting Devices of Rhenium(I) Carbonyls Incorporating Functionalized 2,2′:6′,2″-Terpyridines. *RSC Adv.* **2016**, *6*, 56335−56352.

(68) Klemens, T.; Świtlicka-Olszewska, A.; Machura, B.; Grucela, M.; Schab-Balcerzak, E.; Smolarek, K.; Mackowski, S.; Szlapa, A.; Kula, S.; Krompiec, S.; Lodowski, P.; Chrobok, A. Rhenium(i) Terpyridine Complexes − Synthesis, Photophysical Properties and Application in Organic Light Emitting Devices. *Dalton Trans.* **2016**, *45*, 1746−1762.

(69) Klemens, T.; Czerwińska, K.; Szlapa-Kula, A.; Kula, S.; Świtlicka, A.; Kotowicz, S.; Siwy, M.; Bednarczyk, K.; Krompiec, S.; Smolarek, K.; Maćkowski, S.; Danikiewicz, W.; Schab-Balcerzak, E.; Machura, B. Synthesis, Spectroscopic, Electrochemical and Computational Studies of Rhenium(i) Tricarbonyl Complexes Based on Bidentate-Coordinated 2,6-Di(Thiazol-2-Yl)Pyridine Derivatives. *Dalton Trans.* **2017**, *46*, 9605−9620.

(70) Klemens, T.; Świtlicka, A.; Machura, B.; Kula, S.; Krompiec, S.; Łaba, K.; Korzec, M.; Siwy, M.; Janeczek, H.; Schab-Balcerzak, E.; Szalkowski, M.; Grzelak, J.; Maćkowski, S. A Family of Solution Processable Ligands and Their Re(I) Complexes towards Light Emitting Applications. *Dyes Pigm.* **2019**, *163*, 86−101.

(71) Klemens, T.; Świtlicka, A.; Szlapa-Kula, A.; Krompiec, S.; Lodowski, P.; Chrobok, A.; Godlewska, M.; Kotowicz, S.; Siwy, M.; Bednarczyk, K.; Libera, M.; Maćkowski, S.; Pędziński, T.; Schab-Balcerzak, E.; Machura, B. Experimental and Computational Exploration of Photophysical and Electroluminescent Properties of Modified 2,2′:6′,2″-Terpyridine, 2,6-Di(Thiazol-2-Yl)Pyridine and 2,6-Di(Pyrazin-2-Yl)Pyridine Ligands and Their Re(I) Complexes. *Appl. Organomet. Chem.* **2018**, *32*, No. e4611.

(72) Klemens, T.; Świtlicka, A.; Szlapa-Kula, A.; Łapok, Ł.; Obłoza, M.; Siwy, M.; Szalkowski, M.; Maćkowski, S.; Libera, M.; Schab-Balcerzak, E.; Machura, B. Tuning Optical Properties of Re(I) Carbonyl Complexes by Modifying Push−Pull Ligands Structure. *Organometallics* **2019**, *38*, 4206−4223.

(73) Choroba, K.; Maroń, A.; Świtlicka, A.; Szłapa-Kula, A.; Siwy, M.; Grzelak, J.; Maćkowski, S.; Pedzinski, T.; Schab-Balcerzak, E.; Machura, B. Carbazole Effect on Ground- and Excited-State Properties of Rhenium(I) Carbonyl Complexes with Extended Terpy-like Ligands. *Dalton Trans.* **2021**, *50*, 3943−3958.

(74) Aderne, R. E.; Borges, B. G. A. L.; Ávila, H. C.; von Kieseritzky, F.; Hellberg, J.; Koehler, M.; Cremona, M.; Roman, L. S.; Araujo, C. M.; Rocco, M. L. M.; Marchiori, C. F. N. On the Energy Gap Determination of Organic Optoelectronic Materials: The Case of Porphyrin Derivatives. *Mater. Adv.* **2022**, *3*, 1791−1803.

(75) Tyson, D. S.; Luman, C. R.; Zhou, X.; Castellano, F. N. New Ru(II) Chromophores with Extended Excited-State Lifetimes. *Inorg. Chem.* **2001**, *40*, 4063−4071.

(76) Yarnell, J. E.; McCusker, C. E.; Leeds, A. J.; Breaux, J. M.; Castellano, F. N. Exposing the Excited-State Equilibrium in an IrIII Bichromophore: A Combined Time Resolved Spectroscopy and Computational Study. *Eur. J. Inorg. Chem.* **2016**, *2016*, 1808−1818.

(77) Yarnell, J. E.; Chakraborty, A.; Myahkostupov, M.; Wright, K. M.; Castellano, F. N. Long-Lived Triplet Excited State in a Platinum(II) Perylene Monoimide Complex. *Dalton Trans.* **2018**, *47*, 15071−15081.

(78) Walther, M. E.; Wenger, O. S. Energy Transfer from Rhenium(I) Complexes to Covalently Attached Anthracenes and Phenanthrenes. *Dalton Trans.* **2008**, *44*, 6311−6318.

(79) Liyanage, N. P.; Yang, W.; Guertin, S.; Roy, S. S.; Carpenter, C. A.; Adams, R. E.; Schmehl, R. H.; Delcamp, J. H.; Jurss, J. W. Photochemical CO2 Reduction with Mononuclear and Dinuclear Rhenium Catalysts Bearing a Pendant Anthracene Chromophore. *Chem. Commun.* **2019**, *55*, 993−996.

(80) Li, Q.; Guo, H.; Ma, L.; Wu, W.; Liu, Y.; Zhao, J. Tuning the Photophysical Properties of N∧NPt(II) Bisacetylide Complexes with Fluorene Moiety and Its Applications for Triplet−Triplet-Annihilation Based Upconversion. *J. Mater. Chem.* **2012**, *22*, 5319−5329.

(81) Reineke, S.; Baldo, M. A. Room Temperature Triplet State Spectroscopy of Organic Semiconductors. *Sci. Rep.* **2015**, *4*, No. 3797.

https://doi.org/10.1021/acs.inorgchem.2c02160
Inorg. Chem. 2022, 61, 15070−15084

(82) Maria Maroń, A.; Choroba, K.; Pedzinski, T.; Machura, B. Towards Better Understanding of the Photophysics of Platinum(Ii) Coordination Compounds with Anthracene- and Pyrene-Substituted 2,6-Bis(Thiazol-2-Yl)Pyridines. *Dalton Trans.* **2020**, *49*, 13440−13448.
(83) Chen, K.; Hussain, M.; Razi, S. S.; Hou, Y.; Yildiz, E. A.; Zhao, J.; Yaglioglu, H. G.; Donato, M. D. Anthryl-Appended Platinum(II) Schiff Base Complexes: Exceptionally Small Stokes Shift, Triplet Excited States Equilibrium, and Application in Triplet−Triplet-Annihilation Upconversion. *Inorg. Chem.* **2020**, *59*, 14731−14745.
(84) El Nahhas, A.; Cannizzo, A.; van Mourik, F.; Blanco-Rodríguez, A. M.; Záliš, S.; Vlček, A.; Chergui, M. Ultrafast Excited-State Dynamics of [Re(L)(CO)3(Bpy)] n Complexes: Involvement of the Solvent. *J. Phys. Chem. A* **2010**, *114*, 6361−6369.
(85) El Nahhas, A.; Consani, C.; Blanco-Rodríguez, A. M.; Lancaster, K. M.; Braem, O.; Cannizzo, A.; Towrie, M.; Clark, I. P.; Záliš, S.; Chergui, M.; Vlček, A. Ultrafast Excited-State Dynamics of Rhenium(I) Photosensitizers [Re(Cl)(CO)3(N,N)] and [Re-(Imidazole)(CO)3(N,N)]+: Diimine Effects. *Inorg. Chem.* **2011**, *50*, 2932−2943.
(86) Sanasam, B.; Raza, M. K.; Musib, D.; Pal, M.; Pal, M.; Roy, M. Photodynamic Applications of New Imidazo[4,5-f][1,10]-Phenanthroline Oxidovanadium(IV) Complexes: Synthesis, Photochemical, and Cytotoxic Evaluation. *ChemistrySelect* **2020**, *5*, 13824−13830.
(87) Seth, S. K.; Purkayastha, P. Unusually Large Singlet Oxygen (1O2) Production by Very Weakly Emissive Pyrene-Functionalized Iridium(III) Complex: Interplay between Excited 3ILCT/3IL and 3MLCT States. *Eur. J. Inorg. Chem.* **2020**, *2020*, 2990−2997.
(88) Sanasam, B.; Raza, M. K.; Musib, D.; Roy, M. Photochemical and Photocytotoxic Evaluation of New Oxovanadium (IV) Complexes in Photodynamic Application. *J. Chem. Sci.* **2021**, *133*, No. 42.
(89) Klemens, T.; Świtlicka, A.; Kula, S.; Siwy, M.; Łaba, K.; Grzelak, J.; Szalkowski, M.; Maćkowski, S.; Schab-Balcerzak, E.; Machura, B. The Effect of 2-, 3- and 4-Pyridyl Substituents on Photophysics of Fac-[ReCl(CO)3(n-Pytpy-K2N)] Complexes: Experimental and Theoretical Insights. *J. Lumin.* **2019**, *209*, 346−356.
(90) Baldo, M. A.; Lamansky, S.; Burrows, P. E.; Thompson, M. E.; Forrest, S. R. Very High-Efficiency Green Organic Light-Emitting Devices Based on Electrophosphorescence. *Appl. Phys. Lett.* **1999**, *75*, 4−6.
(91) Maroń, A. M.; Szlapa-Kula, A.; Matussek, M.; Kruszynski, R.; Siwy, M.; Janeczek, H.; Grzelak, J.; Maćkowski, S.; Schab-Balcerzak, E.; Machura, B. Photoluminescence Enhancement of Re(I) Carbonyl Complexes Bearing D−A and D−π−A Ligands. *Dalton Trans.* **2020**, *49*, 4441−4453.

https://doi.org/10.1021/acs.inorgchem.2c02160
Inorg. Chem. 2022, 61, 15070−15084